

**ROLE OF ADP RIBOSYL HYDROLASE AND BINDING
ACTIVITIES OF THE ALPHAVIRUS NSP3 MACRODOMAIN IN
VIRAL REPLICATION IN ASTROCYTES**

by
Taewoo Kim

A thesis submitted to Johns Hopkins University in conformity with the requirements for
the degree of Master of Science

Baltimore, Maryland
April 2020

© 2020 Taewoo Kim
All rights reserved

Abstract

Chikungunya virus (CHIKV) is a positive-sense, enveloped, single-stranded RNA virus belonging to the *Alphavirus* genus. Our studies identified that alphavirus nonstructural protein-3 (nsP3) phosphoprotein includes a macrodomain (MD) which binds and removes ADP ribose groups from mono ADP ribosylated substrates. As a post-translational protein modification, ADP ribosylation transfers ADP ribose from NAD⁺ to the targeted protein by ADP-ribosyltransferases known as poly ADP ribose polymerases (PARPs). To determine the role of the alphavirus nsP3 MD (nsP3^{MD}) ADP ribose-binding and hydrolase activities in viral infection, CHIKVs with point mutations in the nsP3^{MD} were generated and used to infect C8-D1A murine astrocytes. The G32S mutant has less binding and hydrolase activities, while the Y114A mutant has more binding but less hydrolase activities, as compared to wildtype (WT). Infection induced little or no ADP ribosylation of proteins in astrocytes, although there was increased interferon-stimulated PARP gene expression. The G32S mutant was less efficient at initiating infection and making replication complexes than WT virus. Production of viral RNA, nonstructural proteins (nsPs), and infectious virus by G32S was decreased compared to WT at early time points. The Y114A mutant was also less efficient at initiating infection but had a higher number of dsRNA positive cells compared to WT. Levels of Y114A RNA, nsPs, and infectious virus were the same or higher compared to WT. However, in contrast to observations for infection in neuronal cells, in astrocytes the nsP3^{MD} mutants made more structural proteins than WT. In addition, CHIKV infection induced production of type I IFN in astrocytes, but, inhibition of type I IFN signaling did not affect virus replication. Therefore, ADP ribosyl hydrolase and binding activities of the alphavirus nsP3 MD are

critical for viral replication in astrocytes as well as neurons, but cellular responses are distinct. To further compare CHIKV-mediated innate immune signaling pathways, NSC34 neuronal cells that do not produce IFN and C8 astrocytic cells that do produce IFN were infected with CHIKV WT. RIG-I like receptors (RLR) and toll-like receptors (TLRs) were tested, and RLRs were identified as the key innate immune pathway inducing type I IFN in astrocytes, but not in neurons.

Primary reader: Dr. Diane E. Griffin

Secondary reader: Dr. Anthony K. L. Leung

Acknowledgments

I would like to express my gratitude and appreciation to my thesis advisor, Dr. Diane E. Griffin for giving me such a wonderful opportunity to work with her. I was really astonished about her passion for research and informing her research to the public. She attended the diverse conferences and came back even during weekends to work on papers and research. I respect her patience and the professional advice that I can finalize my thesis on time. I would like to thank my secondary advisor, Dr. Anthony K. L. Leung, who has been a great collaborator and an outstanding researcher to communicate the most about an nsP3 project outside our lab.

I also like to appreciate all members of Dr. Griffin's lab: Dr. Rachy Abraham, Dr. Shristi Ghimire, Dr. San Suwanmanee, Dr. Nadine Peart, Dr. Elizabeth Troisi, Dr. Jane Yeh, and Debbie Hauer. All of them have given valuable comments and instructions to decide the direction of projects during data conferences and lab meetings. Especially, I want to acknowledge my research mentor, Rachy, who has served as a role model and instructed me on protocols of virus research.

Finally, I want to thank my family for supporting and cheering through my ScM period. My wife, Jiyun Yoon and my son, David Doha Kim were very supportive while I studied and researched the Chikungunya virus even during the weekends and the vacation. My parents, Gil Rea Kim and Yeon Su Shin showed me unconditional love and support. Thank you all for my dream to work on the virus and for my future aspiration to develop a vaccine.

Table of contents

Abstract.....	ii
Acknowledgments.....	iv
Table of contents.....	v
Abbreviations	vii
List of Figures.....	ix
Chapter 1 INTRODUCTION	1
1.1 CHIKV: Epidemiology, Clinical Manifestation, and Neurovirulence.....	1
<i>Epidemiology</i>	1
<i>Clinical Manifestation</i>	2
<i>Neurovirulence</i>	3
1.2 CHIKV: Genome, Structure, and Replication Cycle	7
<i>Genome</i>	7
<i>Structure</i>	8
<i>Replication Cycle</i>	8
1.3 Immune response to CHIKV infections	12
1.4 Alphavirus Neurovirulence: nsP3, Viral MD, ADP Ribosylation, and PARPs	17
<i>nsP3</i>	17
<i>Macrodomain</i>	18
<i>ADP Ribosylation</i>	19
<i>PARPs</i>	20
1.5 Objectives of the Thesis	25
Chapter 2 ROLE OF ADP-RIBOSYLHYDROLASE AND BINDING ACTIVITIES OF CHIKUNGUNYA VIRUS NSP3 ^{MD} IN ASTROCYTIC CELLS	27
2.1 Introduction	27

2.2 Materials and methods	30
2.3 Results	38
2.4 Discussion.....	54
Chapter 3 UNDERSTANDING THE SIGNALING PATHWAYS LEADING TO THE TYPE I INTERFERON RELEASE IN ASTROCYTES, BUT NOT IN NEURONS	57
3.1 Introduction	57
3.2 Materials and methods	60
3.3 Results	64
3.4 Discussion.....	75
Appendix.....	77
A. References	77
B. Curriculum Vitae.....	85

ABBREVIATIONS

ART	ADP-ribosyltransferases
AUD	Alphavirus Unique Domain
BHK-21	Baby Hamster Kidney -21
cGAS	Cyclic CMP-AMP synthase
CHIKV	Chikungunya Virus
CNS	Central Nervous System
CSF	Cerebrospinal Fluid
Cys	Cysteine
DMEM	Dulbellco's Modified Eagle Medium
DNA	Deoxyribonucleic Acid
EEEV	Eastern equine encephalitis virus
HMW	High Molecular Weight
HPI	Hours Post Infection
HVD	Hyper Variable Domain
IFN	Interferon
IRF	Interferon Regulatory Factor
LMW	Low Molecular Weight
Mab	Monoclonal Antibodies
MAR	Monomeric ADP- Ribose
MD	Macrodomain
MEM	Modified Eagle Medium
Met	Methionine

mRNA	messenger Ribonucleic Acid
NK	Natural Killer
NLR	NOD Like Receptor
nsP	Nonstructural Protein
nsP3 ^{MD}	nsP3 Macrodomain
ORF	Open Reading Frame
PARG	Poly ADPr Glycohydrolases
PARP	Poly ADP Ribose Polymerases
PCR	Polymerase Chain Reaction
PRR	Pattern Recognition Receptor
RIPA	Radioimmunoprecipitation Assay
RLR	Rig-I Like Receptor
RNA	Ribonucleic Acid
SINV	Sindbis Virus
TBK	Tank-Binding Kinase
TBST	Tris-Buffered Saline and Tween 20
TLR	Toll-Like Receptor
UTR	Untranslated Regions
VEEV	Venezuelan equine encephalitis virus
WEEV	Western equine encephalitis virus

Lists of Figures

Figure 1.1:	Global Map of the Predicted Distribution of A) <i>Aedes aegypti</i> and B) <i>Aedes albopictus</i>	5
Figure 1.2	CHIKV Cases Reported: Countries and Territories	6
Figure 1.3	Genome Structure of CHIKV	11
Figure 1.4	Replication Cycle of CHIKV	11
Figure 1.5	TLR, RLR, NLR Innate responses.....	16
Figure 1.6	CHIKV Genome and nsP3 Domains	23
Figure 1.7	Macrodomain Structure.....	23
Figure 1.8	PARPs Related Innate Immune Response	24
Figure 2.1	Astrocyte Cell Viability and Infectious Virus Production After Infection with CHIKV WT and nsP3^{MD} Mutants	45
Figure 2.2	Establishment of Infection in Astrocytes by Transfected Viral RNA and Infectious Virus from WT and nsP3^{MD} Mutants.....	45
Figure 2.3	Formation and Amplification of Replication Complexes in Astrocytes Infected with WT and nsP3^{MD} Mutants	46
Figure 2.4	PARP mRNA Expression and ADP Ribosylation of Proteins During CHIKV WT and nsP3^{MD} Mutants Infection in Astrocytes	47
Figure 2.5	Levels of Genomic and Genomic Plus Subgenomic Viral RNA Produced by Astrocytes Infected with CHIKV WT and nsP3^{MD} Mutants	48

Figure 2.6	The nsP Translation upon Infection by CHIKV WT and nsP3^{MD} Mutants in Astrocytes	49
Figure 2.7	Effects of nsP3^{MD} Mutation on Viral Structural Protein Synthesis and Processing in Astrocytes	50
Figure 2.8	Type I IFN Production after CHIKV WT and nsP3^{MD} Mutants Infection of Astrocytes	51
Figure 2.9	Optimization of Concentration of Antibody Concentrations Required for Blocking of type I IFN signaling in CHIKV-Infected C8-D1A cells	51
Figure 2.10	Infectious Virus Produced by CHIKV WT and nsP3^{MD} Mutants upon Type I IFN Blocking in Astrocytes	52
Figure 2.11	Host Translational Shut off in Astrocytes Infected with CHIKV WT and nsP3^{MD} Mutants.....	53
Figure 3.1	Cell Viability and Infectious Virus Produced after CHIKV WT Infection of Astrocytes and Neurons	68
Figure 3.2	Synthesis of CHIKV Proteins by Infected Astrocytes and Neurons	69
Figure 3.3	Type I IFN response by CHIKV-infected Astrocytes and Neurons	70
Figure 3.4	Phosphorylation of IRF3 and IRF7 in Astrocytes and Neurons after CHIKV Infection.....	71
Figure 3.5	RLR Pathway activation by IFN or Poly (I:C) Treatment of Neurons and Astrocytes	72

Figure 3.6	RLR Pathway mRNA and Protein in CHIKV-Infected Astrocytes and Neurons	73
Figure 3.7	Expression of <i>TLR</i> mRNAs by CHIKV-Infected Neurons and Astrocytes	74

CHAPTER ONE

Introduction

1.1 CHIKV: Epidemiology, Clinical Manifestation, and Neurovirulence

Epidemiology

Chikungunya virus (CHIKV) is a member of the *Alphavirus* genus in the *Togaviridae* family (1,2). Alphaviruses are small, spherical, enveloped, and positive sense, single-stranded ribonucleic acid (RNA) viruses (1,2,3). As chikungunya is a mosquito-borne virus, the current expansion of mosquito vectors into new geographical regions brings public health concerns over the world (2,4). The two major mosquito species that transmit CHIKV are *Aedes aegypti* and *Aedes albopictus* and global maps of their distribution show that they are located mainly in tropical and subtropical regions (Fig. 1.1) (5). This distribution matches the countries and territories where chikungunya cases have been reported (Fig. 1.2) (6).

Since the first discovery of CHIKV at Makonde Plateau in 1952 near Tanzania, limited but continuous spillover events from sylvatic cycles into humans in Southeast Asia and Africa have been reported, (7,8) but the routes of transmission were unidentified. However, investigations of two major outbreaks in Kenya and Comoros, confirmed *Aedes aegypti* as the main vector of CHIKV (8). In 2005, CHIKV causing the outbreak on La Reunion island possessed a mutation in the E1 glycoprotein that increased its new vector adaptability (9). Introduction of the E1-A226V mutation facilitated infection of *Aedes albopictus*, a more widespread vector for transmission of CHIKV to human populations (8,10).

While the virus adapted to this additional vector species, human movement, climate changes, and urbanization further exacerbated the spread of CHIKV throughout the world. Human movements associated with trade and travel introduced these vectors to new regions such as Europe and the Americas (11). Climate change with global warming made the temperate climate zone a more suitable tropical region for the reproduction of vectors (11). Simultaneously, urbanization helped anthropophilic *Aedes* species to adapt and spread across the continents (12).

Currently, CHIKV has affected more than 50 countries and 2 million suspected cases have been reported (13). Two countries with recent outbreaks were Brazil and Thailand. Although travel-associated cases occurred, few countries had endemic transmission in 2019 (14). However, as the vectors spread surveillance for CHIKV needs to be maintained.

Clinical Manifestation

The incubation period of CHIKV is usually 2-12 days (15,16) and rates of lab confirmed asymptomatic CHIKV cases ranged from 3.8% to 27.7% (15). These rates of asymptomatic CHIKV are lower than those of the other mosquito-borne viruses (16) although symptoms for many patients are mild. Typically, chikungunya fever is characterized as an abrupt onset of fever, polyarthralgia, and rash with fatigue (16,17). Around 90% of symptomatic cases have polyarthralgia affecting the joints of ankles, wrists, and knees (16,17). A rash on the arms and trunk is another characteristic symptom occurring in around 50% of confirmed cases. The rash is identified within 2-5 days of infection and resolves within 2 weeks (15, 18), but arthritis can become chronic. Virus may persist and induce continuous secretion of IL-6 as well as CHIKV-specific IgG (16,

19, 20). Therefore, most CHIKV infections are not fatal, but patients with other risk factors such as diabetes and cardiovascular diseases can develop more severe disease (15-21, 22).

Neurovirulence

Mutations in the viral genome can result in changes in virus phenotypes, host reservoirs, and tissue tropism leading to altered virulence. During the 2005-2006 Reunion Island outbreak, 25% of patients reported neurologic symptoms (22). While the Old-World CHIKV is not usually associated with encephalitis, some patients developed encephalitis, encephaloneuropathy, Guillain-Barré syndrome, and stroke (23,24). Neurovirulence of this reemerged CHIKV resulted in long term of sequelae of infection that affected the health and well-being of infected patients.

Mechanisms of alphavirus neurovirulence are either through virus-induced cell death or inflammatory damage to the central nervous system (CNS) (25). Most encephalitic alphaviruses do not cause neurologic disease because innate and adaptive immune responses control and clear the virus before brain entry (25). However, when neurotropic viruses replicate in peripheral organs to maintain a high level of viremia, CNS invasion across the blood brain barrier can occur by way of infected leukocytes or cerebrospinal fluid CSF entry (25). In CHIKV-infected patients with neurological disease, virus could be isolated from the CSF, and viral RNA could be amplified by RT-PCR to confirm this potential route of CNS entry (22).

In vivo studies showed that astrocytes are the main target cells for CHIKV in the human brain although oligodendrocytes and neurons are also susceptible to infection (26, 27, 28). Histopathology demonstrated that newly isolated Asian and East, Central, and

South African (ECSA) strains infected mice by traversing the blood-CSF barrier, with localization to astrocytes and neurons (27). The main functions of astrocytes are to maintain homeostasis of the brain and modulate levels of ions, neurotransmitters, and gliotransmitters (29). Because astrocyte end feet are in close contact with endothelial cells of the blood-brain barrier, they are exposed to virus infection (29). Upon infection, if astrocytes cannot clear the virus, they can transmit the virus to other CNS cells that may result in cell death due to apoptosis or necrosis.

In response to CHIKV infection, astrocytes activate the pro-apoptotic gene, eIF2 α K2 (70) to induce apoptosis. *In vitro* studies have demonstrated that CHIKV-infected astrocytes upregulate the mRNA levels of other proapoptotic factors, such as TNF- α , FasL, and lymphotoxin B (28). Astrocytes activate the caspase-9 apoptotic programmed cell death pathway (28). When astrocytes continuously produce virus, proteins are processed for presentation to CD8⁺ T cells as targets for cytolysis (25). Both clearance pathways cause death of unreplaceable infected cells and acute neurological disease. For other alphaviruses, antibody-mediated long-term virus control is necessary to prevent neurologic disease due to reactivation (30). Therefore, it is optimal to clear the virus before it infects the CNS.

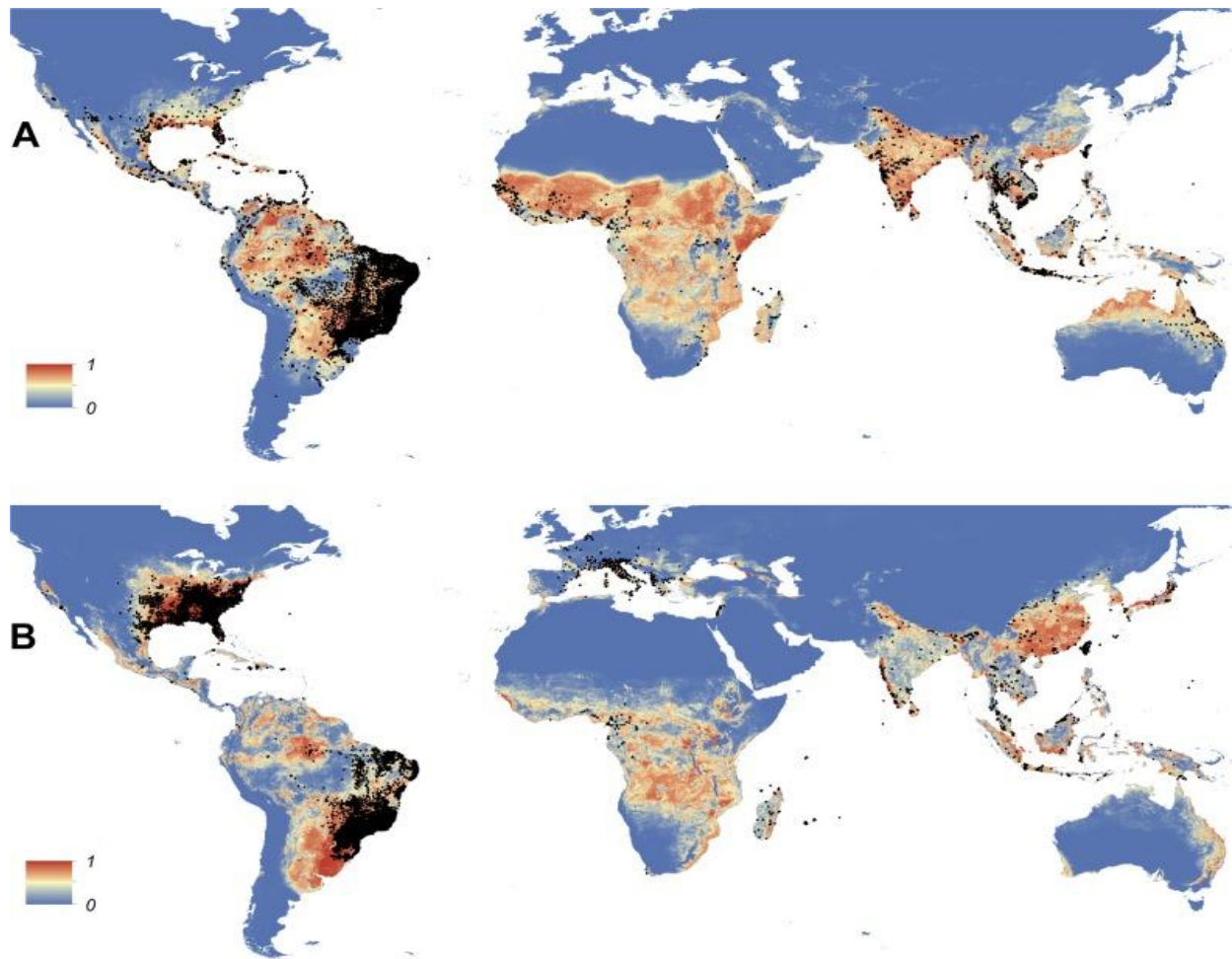


Figure 1.1 Global Map of the Predicted Distribution of A) *Aedes aegypti* and B) *Aedes albopictus*. The colors of the map express the frequency of the distribution, and black dots represent the distribution of the occurrence of each species. Image was adapted from *Kraemer M. UG et al, eLIFE, 2015 (5)*.

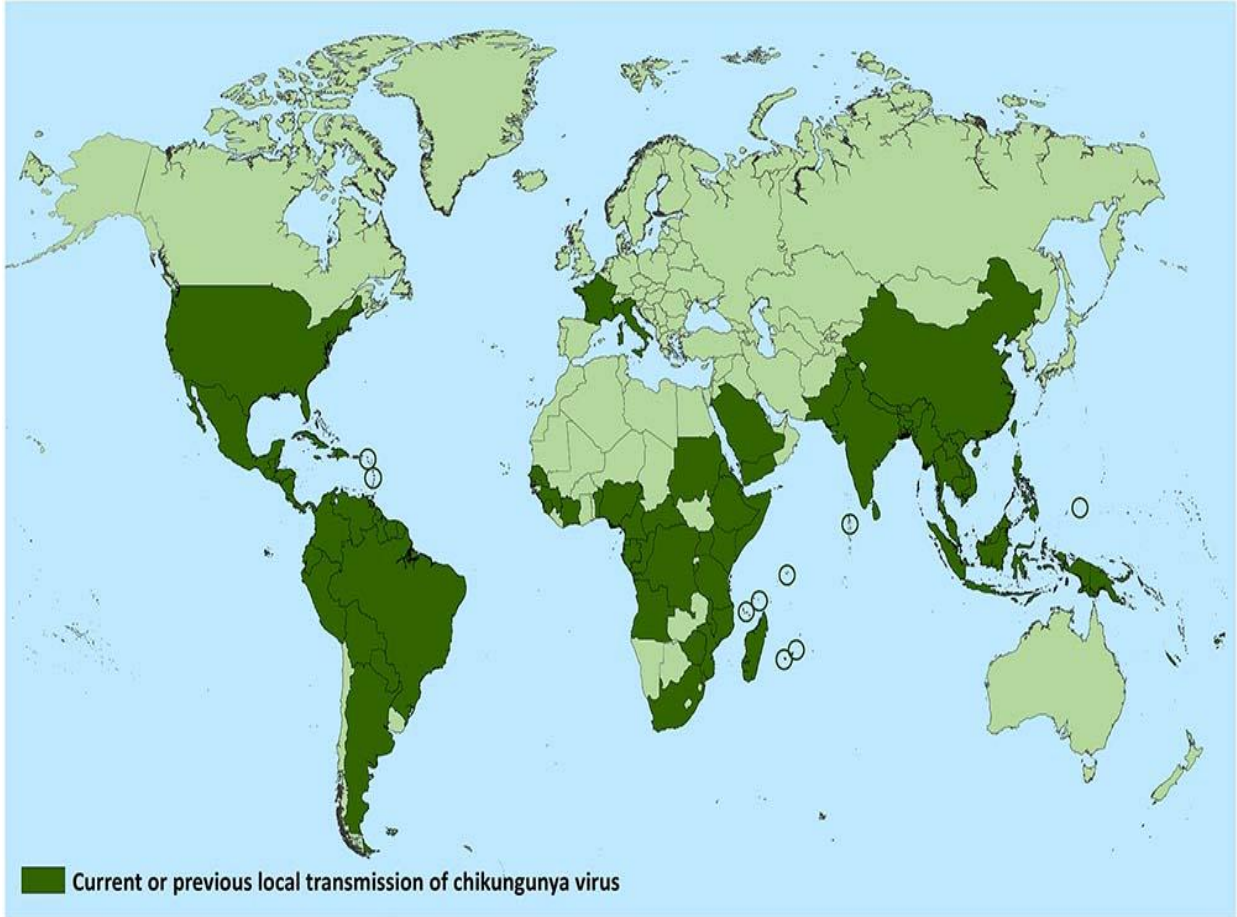


Figure 1.2: CHIKV Cases Reported: Countries and Territories. Geographical distribution of CHIK cases and outbreaks over the world. Countries are mainly located in North and South America, Southeast Asia, Africa, and Southern Europe. The image was adapted from CDC on March 11, 2020 (6).

1.2 CHIKV: Genome, Structure, and Replication Cycle

Genome

CHIKV is a member of the alphavirus family of arthropod-borne, positive-sense, single-stranded RNA viruses (1, 2, 3, 22). Other pathogenic human alphaviruses include Sindbis virus (SINV), western, eastern and Venezuelan equine encephalitis viruses (WEEV, EEEV, and VEEV), and Ross River virus (1, 31). As alphaviruses share common characteristics, important research from other investigators has contributed to our current understanding of the genome, structure, and replication process of CHIKV.

The genome size is about 11,800 bases and composed of two open reading frames (ORFs) (32). The first ORF encodes a polyprotein P1234, which is cleaved into four different non-structural proteins (nsPs) by the autoproteolytic activity of nsP2 to form the fully functional and versatile replicase enzymes required for the replication process (Fig. 1.3) (32, 33). The second ORF as a subgenomic RNA encodes another polyprotein that includes the 3 main structural proteins (capsid, E1, E2) and three small peptides (E3, TF and 6K) (32,33,34).

There are 5' and 3' untranslated regions (UTR) and a junction between the two ORFs. The lengths of the 5' UTRs differ among alphaviruses. The 5' end has a type 0 5' cap structure (N7mGppp) to stabilize the virion genome and facilitate translation of viral proteins for replication (35). The 5' UTR is recognized by host translational factors (eIF4E and eIF4F) to form the distinct secondary structure for translation of the nonstructural polyprotein (35). The 5' UTR of the subgenomic RNA does not require eIF4G or eIF2 for translation initiation of the structural proteins and thus escapes host-translation shut off by PKR activation as part of the innate immune response (35,36). At the 3' end, there is

a poly (A) tail to support negative strand RNA synthesis and efficient translation (35). At least 11-12 residues are required in the 3'UTR to interact with the RNA recognition motifs of poly (A)-binding protein (36). Like the 5' UTR, the length of the 3' UTR for each alphavirus is different. While host cellular miRNA targets 3' UTR of CHIKV as an immune response, CHIKV can adapt to evade the cellular response with mutations in the 3' UTR regions selected to eliminate binding sites (35, 37).

Structure

Numerous research projects have studied 3D structures of alphaviruses through cryogenic electron microscopy and crystallization of component proteins since the 1990s (1). Based on recent studies with more advanced technologies, one copy of the 11.8Kb genome and surrounding capsid proteins form icosahedral nucleocapsid structures to protect its viral RNA. These structures are covered by an envelope containing glycoproteins embedded in a lipid bilayer (1). For each virion 240 Immature E1 and pE2 glycoprotein heterodimers are synthesized in the endoplasmic reticulum within the lipid bilayer (38). Between the pE2 and E1 heterodimer, there are 6K proteins to regulate ion permeability between the environment and the virus (39). As viroporins, 6K proteins help virus release through budding and membrane permeability at the host cell plasma membrane (39). Host furin cleaves pE2 into E2 and E3 during Golgi transport (40). E1 and E2 heterodimers form mature trimeric spikes at the virus surface. The E1 glycoprotein is responsible for the fusion of virus membrane and host membrane, while E2 glycoproteins bind host receptors and stimulate receptor-mediated endocytosis (1, 40).

Replication Cycle

Most alphaviruses utilize E2 glycoproteins for binding to host receptors and receptor-bound virus particles are predominantly internalized through clathrin-mediated endocytosis (Fig. 1.4) (13, 41). siRNA screening in the human osteosarcoma U2OS cell line demonstrated that the silencing of clathrin blocked CHIKV entry (42). During virus binding, glycosaminoglycans and TIM1 within the host membrane work as attachment factors (13, 41). As glycosaminoglycans are present in most cell types, CHIKV does not show cell type-specificity (13) and even without known attachment factors, CHIKV still can infect many types of host cells.

CHIKV fusion with endosomes is cell type-dependent. In C6/36, a mosquito cell line (*Ae. albopictus* salivary gland), CHIKV fuses with both Rab5-positive early endosomes and Rab7-positive late endosomes (41, 43, 44). However, in HEK 293T human epithelia cells, CHIKV fusion is dependent only on early endosomes (44). Because of conformational changes at low pH, the virus envelope and endosomal membrane fuse and deliver the virus genome into the cytoplasm (13). The virus genome is directly translated by hijacking host translation factors to synthesize a polyprotein nsP1234 followed by regulated nsP2 cleavage of the polyprotein to nsP1, nsP2, nsP3, and nsP4 (13). As nsP4 is the RNA dependent RNA polymerase, all replicase enzymes assemble with the viral genome to recruit host factors and form RNA replication complexes (45). Following synthesis of newly made positive-sense viral RNA, RNA replication complexes exponentially increase until all cytosolic host factors are in use for viral RNA replication (45). The dsRNA intermediates within RNA replication complexes are surrounded by a double membrane spherule to evade detection by the host innate immune response (13,45). When adequate numbers of nsPs are transcribed and translated, translation of

subgenomic RNA (2nd ORF) for the synthesis of the structural polyprotein begins (45). Capsid is autocatalytically cleaved from the glycoproteins that are then processed by host enzymes in the ER. Post-translational modification, such as palmitoylation and glycosylation matures E1 and pE2 heterodimers into fully developed spikes (13). Furin cleaves pE2 between E3 and E2 in the Golgi (13). There are two ways for CHIKV to be released from infected cells. First, the spikes are delivered to the plasma membrane, and nucleocapsids interact with the envelope spikes to bud out directly to the extracellular space (46). Second, capsids and spikes can be assembled within vesicles and delivered extracellularly as an exosome (46).

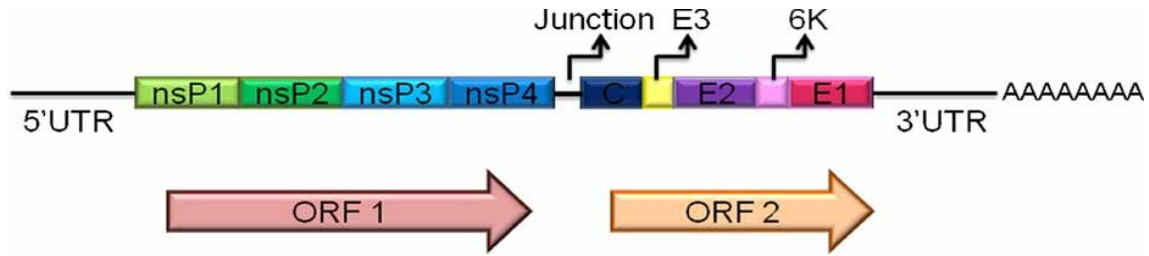


Figure 1.3: Genome Structure of CHIKV. The CHIKV genome includes two open reading frames, a 5' cap, and a 3' poly (A) tail. Genomic mRNA and subgenomic mRNAs are produced. Genomic mRNA is translated to produce a polyprotein that is cleaved into four non-structural proteins (nsP1, nsP2, nsP3, and nsP4). Subgenomic mRNA encodes five structural proteins: capsid, two glycoproteins (E2 and E1), and three small peptides (E3, TF and 6K). The image is adapted from *Singh, S. K., & Unni, S. K., Medical Virology, 2015 (32).*

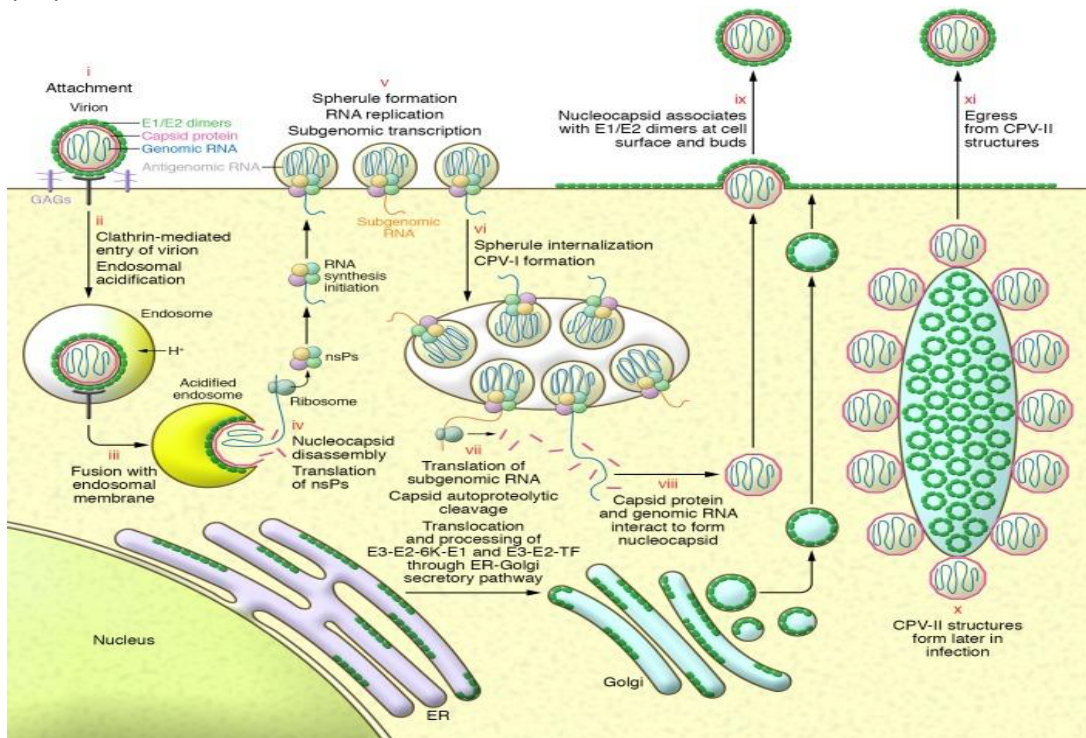


Figure 1.4: Replication Cycle of CHIKV. CHIKV E2 proteins bind host cell receptors and clathrin-mediated endocytosis brings the virion into the cell. Low pH in acidified early endosomes induces a conformational change in the glycoprotein spikes and fusion of E1 proteins with the endosomal membrane to deliver the viral genome to the cell cytoplasm. After the translation of nsPs from genomic RNA, replication complexes are formed at the plasma membrane to produce viral RNAs. Subgenomic RNA is translated to produce the structural proteins required to assemble new virus particles. After packaging, viruses either bud out or egress out as a large vesicle. The image is adapted from *Silva, L. A., & Dermody, T. S., The Journal of clinical investigation, 2017 (13).*

1.3 Immune response to CHIKV infections

Host antiviral defenses include the innate and the adaptive immune responses (47). The mammalian innate immune response is initiated by sensing the presence of the virus. It both inhibits viral replication and alerts the adaptive immune response (47). Both type I interferon and inflammatory cytokines play important roles in the innate immune response. The mammalian adaptive immune response targets specific viral antigens and involves the participation of dendritic cells, T cells, and B cells (48). Specific immunoglobulins, cytokines and effector activities of B and T cells are the main results of adaptive immune responses (48).

Pattern recognition receptors (PRRs) are the frontline of innate immune response recognition of pathogen-associated molecular patterns to sense the existence of the virus. PRRs can be either immune sensing receptors or sensing and effector receptors (49). Immune sensing receptors are Toll-like receptors (TLRs), RIG-I like receptors (RLRs), NOD-like receptors (NLRs) and cyclic CMP-AMP synthase (cGAS) that sense viral genomes or proteins. After cell entry at the endosome, endosomal TLRs (TLR3, 7, 8, and 9) can recognize dsRNA, ssRNA, and CpG DNA viral genomes (49). TLR2 and 4 can also detect viral structural proteins at the plasma membrane and activate the adaptor protein TIRAP (50). All TLRs except TLR3 signal through the MyD88 and TRAF6 pathway to activate NF κ B (84). TLR3 signals through its own TRIF/TRAM pathway to phosphorylate interferon regulatory protein (IRF) 7 to activate both IFN and NF κ B pathways (50).

Both intracellular MDA5 and RIG-I RLRs are RNA helicases recognizing long dsRNA and 5'triphosphate RNA, which are unusual molecules in uninfected cells.

Following RNA recognition, RLRs interact with MAVS as its adaptor protein and activate tank-binding kinase 1 (TBK1) to phosphorylate IRF3 early and activate both IRF3 and IRF7 at later time points. Activation of IRF3 and IRF7 induces production of mRNA for type I IFN. NLRs can recognize ssRNA to cause inflammasome and caspase 1 activation (49, 51). NLRP3 induced through the NF κ B pathway and pro IL1 β form inflammasomes that can activate caspase 1 to release IL1 β and IL18 (49). cGAS can recognize viral DNA in the cytosol and interact with STING to activate TBK and the IFN producing pathway (48).

Protein kinase PKR is a sensing and effector receptor binds to long viral dsRNA and phosphorylates translation initiation factor eIF2 α . eIF2 α is a recyclable protein translation factor but, phosphorylation prevents reuse and thus inhibits protein translation (51). This inhibition is efficient for both viral and cellular protein translation unless viral evasion mechanisms exist.

RLRs, TLRs, and PKR are the main receptors detecting CHIKV ssRNA and dsRNA (Figure 1.5) (50). TLR7 and 8 can recognize viral positive ssRNA to activate the Myd88/TRAF6 pathway and phosphorylate IKK β and I κ B. NF κ B signaling controls mRNA transcription for production of antiviral cytokines (48, 51). TLR3 can recognize CHIKV intracellular dsRNA produced by replication complexes. Recognition of dsRNA can activate both type I IFN and NF κ B pathways. In animal studies, TLR3 knockout mice infected with CHIKV had increased viremia, infected macrophages and neutrophils, and reduced CD4⁺ T cells (85). Therefore, TLR3 is involved with recognition of virus and reduction of viremia.

Both intracellular MDA5 and RIG-I RLRs limit CHIKV replication and initiate type I interferon production, mainly IFN β at early time points (47). IRF3 is the initial regulator of anti CHIKV responses downstream of RLRs. Phosphorylation and activation of IRF3 results in the induction of immediate early IFN mRNA and synthesis of IFN β . Early IFNs can act in an autocrine or paracrine manner to induce synthesis of more IFN β , IFN α , and antiviral proteins (48). Type I interferon receptors signal to synthesize and activate IRF7. Activated IRF7 and IRF3 together induce synthesis of more antiviral proteins (48, 49). Without IRF7, CHIKV-infected mice could not induce type I IFN, and type I IFNs were not detected in serum (53). IFN α and IFN β (together as Type I IFN) bind to cell surface receptors to activate the JAK/STAT pathway to induce expression of IFN-stimulated genes (ISGs) (54). Two host defense ISGs against CHIKV infection are major histocompatibility (MHC) class I and ISG15. When more MHC class I proteins are synthesized in the endoplasmic reticulum, more processed viral peptides bind to MHC class I and are transported to the cell surface to interact with CD8⁺ T cells (54). ISG15 inhibits viral release by blocking virus budding (55). ISG15 knockout mice are more susceptible to CHIKV with increased mortality (56). Thus, for early detection of CHIKV, type I IFN is an essential element of the innate immune response.

For the innate cellular immune responses, upon CHIKV infection, astrocytes produce inflammatory chemokines CCL2 and CCL7 in response to NF κ B-induced IL1 β and TNF α (57). CCL2 and CCL7 recruit macrophages to replication sites where they produce IL6, TNF α and GM-CSF to counter CHIKV infection. Another type of recruited macrophage expresses M2-associated proteins to help tissue repair for apoptosis but also can become a reservoir for CHIKV (57). Natural killer (NK) cells are also recruited to

CHIKV-infected tissues to produce perforin and cause cytolysis before CD8⁺ T cells arrive at the site (57). NK cells also secrete IFN γ and TNF α to activate macrophages and induce more Class II MHC to bridge innate and adaptive immune responses.

The adaptive immune response to CHIKV infection can both protect and destroy host cells. In mouse models as virus titers reach peak levels, within 7 days CD8⁺ T cells come to infected sites (58). However, knock out of CD8⁺ T cells did not increase CHIKV viremia or the degree of subcutaneous disease compared to WT demonstrating that CD8⁺ T cells did not efficiently clear virus, but rather caused death of infected cells. CD4⁺ T cells contributed significantly more to reduction of viremia and disease (57, 58). The most effective adaptive immune response to eliminate circulating infectious CHIKV was antibody. Antibody neutralizes CHIKV by binding to the trimer spikes of glycoprotein heterodimers (57). Both innate cellular immune response and adaptive immune responses inefficiently destroy host cells causing subcutaneous and neurologic disease. Therefore, inducing Type I IFN is extremely important for early detection of virus leading to antibody production.

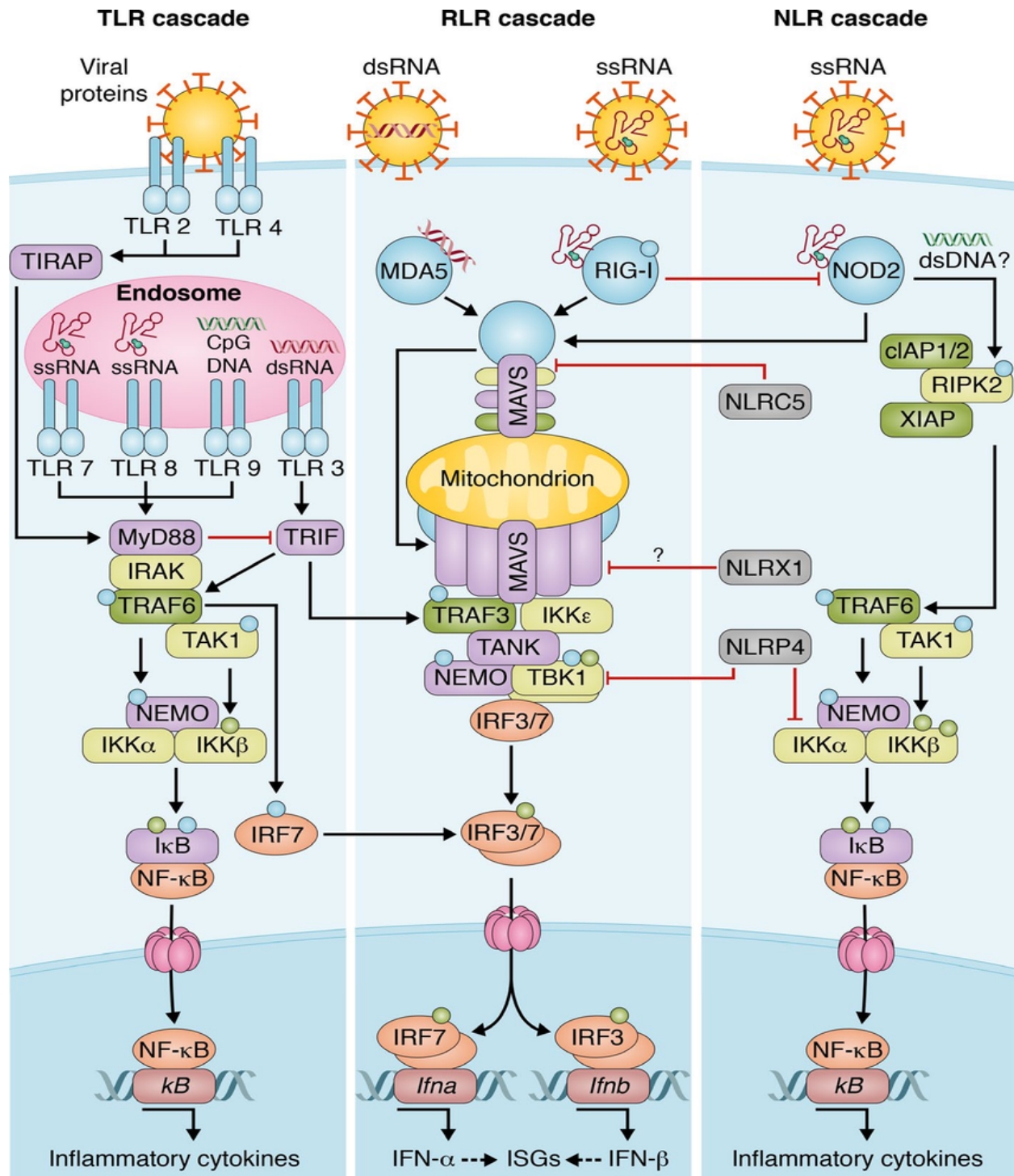


Figure 1.5 TLR, RLR, NLR Innate responses. For antiviral defense, host cells have innate immune response signaling pathways. RLRs and TLRs are the main innate immune pathways that induce transcription of the type I IFN gene. After translation of type I IFN, interferon stimulated genes are produced that inhibit virus replication within cells. (50) The image is adapted from *Heaton, S. M., Borg, N. A., & Dixit, V. M., JEM, 2016 (50).*

1.4 Alphavirus Neurovirulence: nsP3, Viral MD, ADP Ribosylation, and PARPs

nsP3

The first ORF of CHIKV encodes 4 nonstructural proteins. nsP1 is an RNA capping enzyme with N-7methyltransferase and guanylyltransferase functions that protect the viral genome from degradation by host nucleases (59,60). nsP2 has helicase and protease activities. When dsRNA is made during replication and transcription, nsP2 unwinds dsRNAs for further use. Simultaneously, nsP2 can cleave the viral nonstructural polyprotein into several functional replicase enzymes (1,13, 61). nsP4 is an RNA dependent RNA polymerase for the replication. However, the function of nsP3 is more enigmatic and it is the least understood of the nsPs.

Within alphaviruses, the size of nsP3 proteins range from 469 to 570 residues (62). nsP3 is composed of three different domains. Starting with N terminus, they are the macrodomain (MD), the alphavirus unique domain (AUD) (central zinc-binding domain), and the hypervariable domain (HVD) (Fig. 1.6). HVD is the most well-characterized and has the most variable sequences (62). One function of the CHIKV HVD is interaction with the Ras-GAP SH3 domain-binding protein (G3BP) 1 and G3BP2 to form stress granules (63). Initially, nsP3 is located within the replication complexes and later interacts with G3BP1 and G3BP2 (64,65,66). Stress granules can have both anti- and proviral activities (63). Viruses modulate stress granules to sequester their viral RNA with cell components and increase the replication efficiency (67). On the other hand, cells can recognize the existence of viral RNA with intracellular innate responses before viral protein translation and sequester translation initiation factors into the stress granules before viral proteins can be translated (67).

Function of the zinc-binding domain, also known as the AUD, is poorly understood but has roles in genome replication (62). Viable AUD mutants cannot form normal replication complexes (62). AUD is connected to the MD by a linker to form a circle-like shape (62).

Macrodomain

Macrodomain is a conserved protein fold that consists of 130-190 amino acids with a central beta-sheet enclosed by 4-6 alpha helices (68). MD was first identified in viruses as X-domains and renamed MD when it was recognized as the C terminal domain of histone macroH2A (68). This structure supports binding and processing of nucleotides and its active site accommodates ADP ribose (ADPr) and its derivatives. The active site center binds to the substrate and has two binding-loops (69). Loop 1 is the catalytic loop associated with hydrolase activity (68, 69), and loop 2 is the pyrophosphate-binding loop that further arranges substrate binding (Fig. 1.7) (68).

The diverse functions of the MD are associated with the NAD⁺ signaling pathway, DNA repair mechanisms, redox balance, and response to viral infection (69). To rebuild NAD⁺ for signaling, the MDs interact with NUDIX pyrophosphatases to recycle ADPr into AMP and ribose-5-phosphate (69,70). The MDs of polynucleotide kinase and polyphosphate hydrolase are associated with single-stranded DNA repair (69). While PARP1 adds ADPr after sensing DNA-damage, Poly-ADR glycohydrolases (PARG) can reverse poly ADPr gene regulation. Diverse proteins with MDs help cells to maintain homeostasis.

Macrodomains are conserved and found in all kingdoms of life. The viral MDs are found in a subset of positive sense ssRNA viruses in the families Myoviridae,

Coronaviridae, Togaviridae, and Hepesviridae (69, 70). The MDs of these virus families are in the macro D subclass and found in nsP3s. Viral MDs have two main functions important for virus replication and neurovirulence. They can dephosphorylate and deacetylate monomeric ADP-ribose (MAR) and its derivatives (68,71) and can bind and hydrolyze an ADP-ribose unit from MARylated proteins or the last ADP-ribose from poly ADP-ribosylated proteins (68,72,73,74). Mutations introduced to ADP-ribose binding sites did not affect replication in a non-neuronal cell line, but impaired replication in neuronal cells *in vitro*, and decreased neurovirulence for mice *in vivo* (72,73,74,75). Also, in alphavirus-induced encephalomyelitis, mutations affecting binding and hydrolase activities resulted in less virus replication and less clinical disease in mice (75).

ADP-ribosylation

ADP-ribosylation is a reversible post-translational modification with roles in signaling pathways, gene regulation, DNA repair, and apoptosis (76, 77). As a reversible modification, diverse enzymes regulate this protein modification and are described as writers, erasers, readers, and feeders of ADPr (78, 79). As ADP-ribose writers, ADP-ribosyltransferases (ARTs) and poly (ADP-ribose) polymerases (PARPs) are the main enzymes to deliver mono or poly ADP-ribose units to substrates (76) and have roles in chromatin regulation, stress responses, viral infections and cancer (69). Substrates are not limited to proteins but also can be nucleotides, and any small biological molecules (76). The main target amino acids for ARTs and PARPs have either electrically charged or polar side chains (mainly arginine, lysine, aspartic acid, glutamic acid, serine, and asparagine) (76,77). PARG, ADPr hydrolase, MacroD1 and D2 subclasses of MDs are erasers of ADPr, some of which can hydrolyze ribose-ribose bonds and ester bonds

between ribose and negatively charged amino acids (80). Loss of eraser functions cause cell death and increase sensitivity to stress from DNA damage and pathogens (79).

As ADP-ribose readers, the ADPr binding domain (ARBD) can bind to various forms of ADP ribose on substrates. MDs, PAR-binding domains, and PAR-binding zinc finger motifs are examples of ARBD (78). These ARBDs can identify ADP ribose monomers, junctions between PAR, and ADP-ribose oligomers. By reading the substrates of ADPr, domains can connect ADP-ribosylation and cellular events by recruiting new enzymes (78). NAD⁺ synthases are the feeders of ADPr and produce NAD⁺ from nicotinamide mononucleotide and ATP (78). Partners with PARP, NAD⁺ synthases have defined subcellular localizations, and PARPs recruit the synthases to substrates to receive NAD⁺ for their functions.

PARPs

Humans encode 17 PARPs, and enzymatically active PARP can either MARylate or PARylate target proteins. PARP1 and PARP2 function in DNA repair related to damaged bases and double strand breaks (78, 80) and, in response to cellular stress, these PARPs can initiate parthanatos (80). Both PARPs also respond to metabolic stress related to obesity and cancer (80). *PARP1* and *PARP2* knockout mice were tested for metabolic effects important for homeostasis (80). PARP1 deficiency aggravated diet-induced and age-specific obesity (81). *PARP2* knockout mice had elevated energy and oxygen consumption, lipid oxidation, and were protected from obesity (80).

PARPs are also involved in RNA biogenesis, processing, and trafficking (78, 82). During stress, RNA-rich stress granules are formed to control translation and mRNA stability (82). Regulation of stress granules by PARP5a, PARP12, PARP13.1, PARP13.2,

PARP14, and PARP15 was required to repress translation and degrade mRNA (78, 82). Ribosomal RNA synthesis is also linked to PARP activity. PARP1 binds TIP5 of newly synthesized chromatin and inhibits the ribosomal RNA genes from forming repressive heterochromatin (78). In drosophila, PARP can bind to rRNA transcription and help maintain the structural integrity of nucleoli (78).

While PARP1 and PARP2 are poly PARP enzymes, PARP6, PARP10, and PARP16 are mono PARP enzymes used in diverse signaling pathways. During neurodevelopment, PARP6 is a regulator of hippocampal neuron development (83). While newly developed neural circuits were dependent on dendrite growth and branching, PARP6 promoted complexity during dendrite morphogenesis (83). PARP10 is a repressor of the NF κ B pathway. PARP10 not only prevents polyubiquitination of NEMO but also ADP-ribosylates NEMO (83). Therefore, PARP10 inhibits nuclear localization of NF κ B. PARP16 is the main enzyme to induce an unfolded protein response at the endoplasmic reticulum by controlling UPR pathways related to endonucleases (83).

While PARPs have diverse cellular functions, some PARPs also have innate immune response antiviral activities (84). PARP13, the first known antiviral family member, degrades retroviral RNA and promotes TRAIL-mediated apoptosis in response to viral infection (85, 86). PARP family members also regulate interferon, a fundamental innate immune response. PARPs 1, 9, 12, 13, and 14 either promote expression of type I IFN or interferon-stimulated genes (ISGs) (Fig. 1.8) (87). PARP1 promotes NF κ B activation in macrophages. CHIKV uses macrophages as carriers to transmit virus to different cell types and activate NF κ B to induce proinflammatory cytokines (87). PARP9 interacts with transcriptional factors to remodel chromatin and increase the expression of

certain ISG genes (87). PARP12 binds to the TLR3 adaptor protein TRIF to enhance NF κ B pathway gene expression (87). PARP13 can bind to the RLR downstream protein MAVS to initiate pathway activation (87), and PARP14 promotes IFN promoter acetylation to enhance Pol II binding (87). However, PARP10 has proviral activity and indirectly improves virus replication by increasing cell survival through the NF κ B pathway (87).

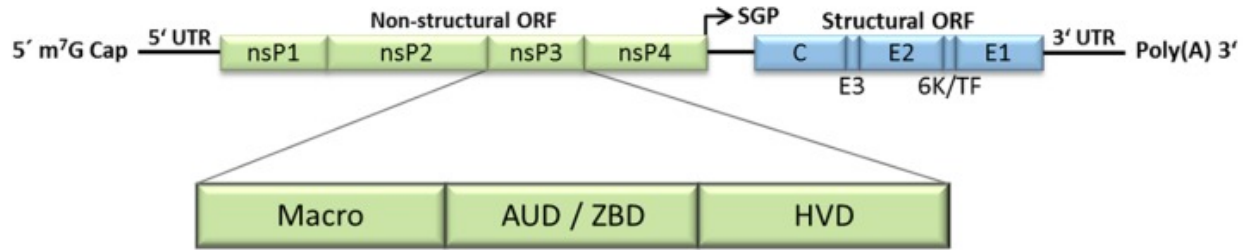


Figure 1.6: CHIKV Genome and nsP3 Domains. nsP3 has three major domains: a highly conserved N-terminal macrodomain, a central zinc-binding region, and a poorly conserved highly phosphorylated C-terminal domain. The HVD interacts with many cellular proteins for virus replication and stress granule assembly, but the roles of the macrodomain and zinc-binding domain are less well characterized. The image is adapted from Götte, B., Liu, L., & McInerney, G. M, *Viruses*, 2018 (62).

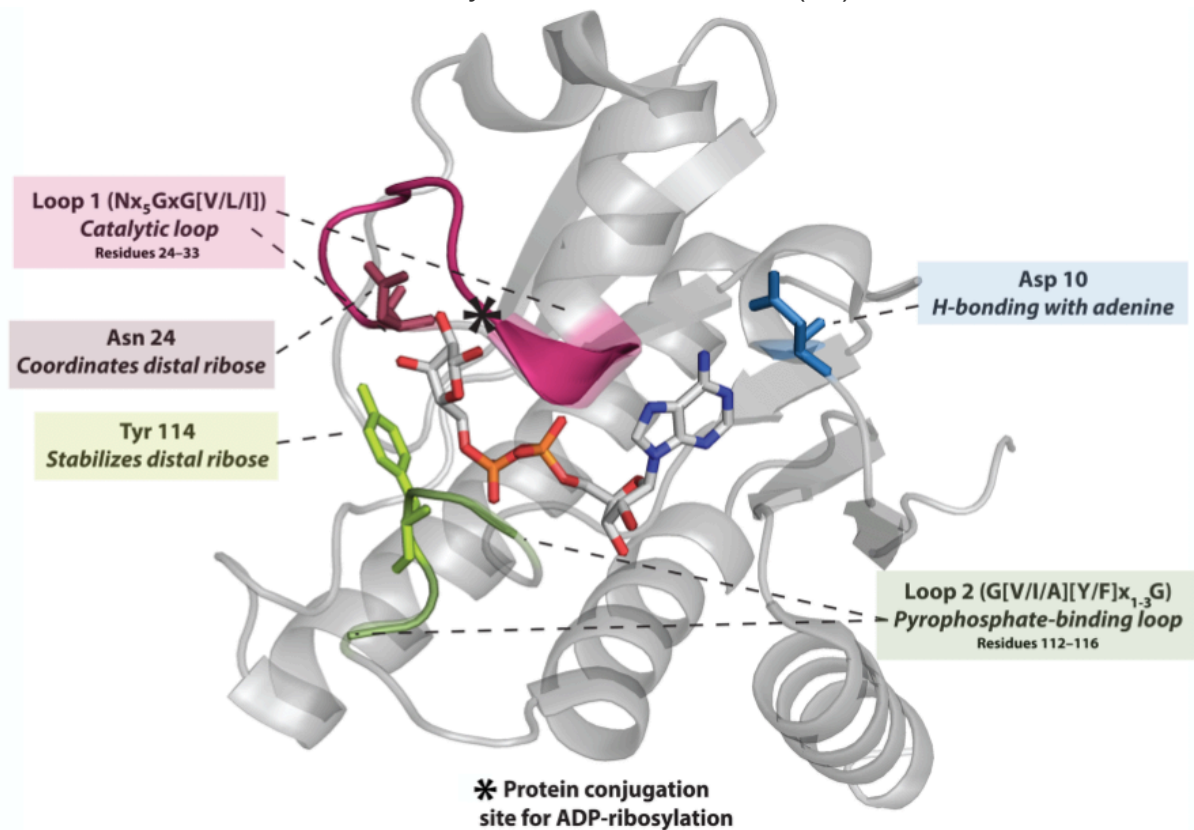


Figure 1.7: Macrodomain Structure. Macrodomain has a central beta sheet surrounded by 4-6 alpha helices. The center of the active site can bind to the side chain of the substrate. Two loops are associated with MD function. Loop 1 (catalytic loop) has hydrolase activity, and loop 2 (pyrophosphate-binding loop) stabilizes binding. The image is adapted from Leung, A., McPherson, R. L., & Griffin, D. E., *PLOS Pathogens*, 2018 (68).

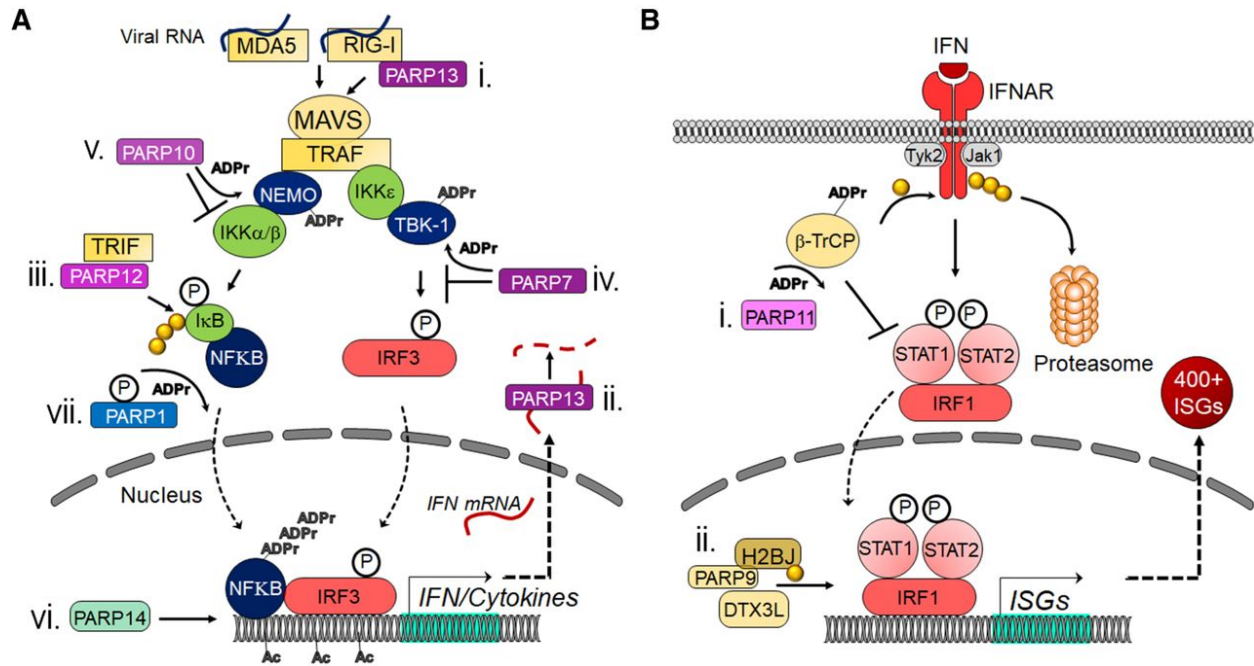


Figure 1.8: PARPs Related Innate Immune Response. (A and B) PARP 1, 9, 12, 13, 14 are antiviral PARPs related to the innate immune response with activation of type I IFN, ISG and NFκB pathways. However, PARP7, 10, and 11 demonstrate proviral properties. The image is adapted from *Fehr, A. R., Singh, S. A., Kerr, C. M., Mukai, S., Higashi, H., & Aikawa, M., Genes and Development, 2020 (87).*

1.5 Objectives of the Thesis

Macrodomains (MD) are highly conserved protein folds that bind ADP ribose (ADPr). ADP ribosylation is a post-translational protein modification resulting from transfer of ADPr from NAD^+ to substrates by ADP-ribosyl transferases known as poly ADP ribose polymerases (PARPs). Our lab previously identified that the MD of the alphavirus nonstructural protein-3 (nsP3) phosphoprotein not only binds but also removes ADPr groups from mono ADPr substrates, and that this hydrolase activity is necessary for viral replication in cells and virulence in mice (72). Also, studies of neuronal cells confirmed that ADP ribosylation of proteins and nsP3^{MD} ADPr binding are necessary for initiation of alphavirus replication, while hydrolase activity facilitates amplification of replication complexes (73).

Histopathology studies of CHIKV infection in a mouse model show that within the brain CHIKV preferentially infects astrocytes, ependymal cells, epithelial cells of the choroid plexus and neurons (28). There is increased expression of interferon-stimulated PARP mRNAs upon alphavirus infection in CNS tissues of mice and in astrocytic cells, whereas in neuronal cells PARP activation occurs to drive ADP ribosylation of proteins without increased mRNA expression. The main objective of this research project was to understand how the ADP ribosyl binding and hydrolase activities of CHIKV nsP3^{MD} affects CHIKV replication in astrocytes, and how astrocytes differ from neurons in the induction or production of type I IFN.

Objective 1: Determine the importance of CHIKV nsP3^{MD} ADP ribosyl hydrolase and binding activities for viral replication in astrocytic cells.

Objective 2: Compare the responses to CHIKV infection of astrocytes (produce IFN) and neuronal cells (do not produce IFN) that determine the type I IFN response.

CHAPTER TWO

Role of ADP-ribosyl hydrolase and binding activities of chikungunya virus nsP3^{MD} in astrocytic cells

2.1 Introduction

Chikungunya virus (CHIKV) is an enveloped, positive sense ssRNA Old World alphavirus, which is transmitted by mosquito vectors (1, 3). While CHIKV mainly causes rash and arthritis accompanied by fever, re-emerging strains in recent outbreaks have also caused encephalitis and other neurological diseases (15, 17). *In vivo* studies demonstrated that newly isolated CHIKV strains preferably traverse the blood-CSF barrier to infect the brain, with viral proteins localized in astrocytes and neurons (26, 27, 28). Astrocytes are specialized glial cells with diverse functions including formation of the blood-brain barrier structure, nutrient support to neurons, glutamate transport, and regulation of synaptic transmission (88). Astrocytic end feet are connected to endothelial cells of the blood-brain barrier and available for infection by CHIKV. CHIKV-infected astrocytes can activate defensive cell death pathways and CD8⁺ T cells can kill infected cells through Fas-Fas ligand signaling to prevent virus spread (88). Death of unreplaceable neurons during CHIKV infection causes acute neurological damage . However, the molecular mechanisms of CHIKV neurovirulence mediated mainly through astrocytes is poorly characterized.

The 11.8kb genome of CHIKV encodes four nonstructural proteins and five structural proteins. The nonstructural proteins form the replication machinery and synthesize genomic and subgenomic RNA necessary for virus production (72). nsP1 is an RNA capping enzyme to protect the viral RNA and facilitate translation (59). nsP2 has

helicase and protease functions to unwind dsRNA during the replication and cleave the nonstructural polyprotein into individual proteins (1,13). nsP4 is an RNA-dependent RNA polymerase for synthesis of viral RNA. nsP3 is a phosphoprotein with ADPr-binding and hydrolase activities that help to establish and amplify replication complexes (72, 73, 74). nsP3 also disrupts stress granules to release translation initiation factors and increase virus production (63, 67). nsP3 is a determinant of neurovirulence, induces the formation of spherules at the plasma membrane and controls RNA synthesis in replication complexes (72, 74).

Macrodomains (MD) are highly conserved protein folds that bind ADP ribose (ADPr). ADP ribosylation is a post-translational protein modification resulting from transfer of ADPr from NAD⁺ by ADP-ribosyltransferases known as poly ADP ribose polymerases (PARPs) (68). Viral MDs are in the macro D subclass and highly conserved in nonstructural protein 3 of the coronavirus and togavirus/alphavirus families of positive-sense RNA viruses. The first identified function of viral MDs was dephosphorylation and deacetylation of MAR and its derivatives (68). Another function includes binding and hydrolysis of ADPr from MAR proteins (68, 72, 73, 74) important for virus replication and neurovirulence. MDs of alphaviruses hydrolyze the ester bonds between ribose and negatively charged amino acids (78). Mutations in the two functional loops of the alphavirus MD resulted in less virus replication in neuronal cells and decreased neurovirulence in mice (72, 73, 74, 75).

Earlier studies determined the roles in viral replication of the ADPr-binding and hydrolase activities of the alphavirus nsP3 MD (nsP3^{MD}) in neuronal cells. ADP ribosylation of proteins and nsP3^{MD} ADPr binding are necessary for initiation of alphavirus

replication, while hydrolase activity facilitates amplification of replication complexes (73). Both activities were also important determinants of the outcome and pathogenesis of alphavirus encephalomyelitis in mice. Compared to the WT, the virus mutant with decreased hydrolase and binding activities replicated less well in both the brain and spinal cord, induced similar innate responses, and caused less severe disease with full recovery of survivors, whereas the virus mutant with better binding activity, but less hydrolase activity replicated well, induced higher expression of interferon-stimulated and NF- κ B-induced genes, and was cleared more slowly from the spinal cord with persistent paralysis in survivors (74).

While recent studies mainly focused on murine neuronal cells *in vitro* and demonstrated a role in the pathogenesis of alphavirus encephalomyelitis in mice (72,73), in the present study we seek to determine the role of ADPr-binding and hydrolase activities of alphavirus nsP3^{MD} in viral replication in astrocytes, the preferred target cells for CHIKV in brain.

2.2 Materials and Methods

Cell Culture

Murine astrocytic C8-D1A (astrocyte type I clone), baby hamster kidney 21 (BHK 21), and African green monkey epithelial (Vero) cells from American Type Culture Collection (ATCC) were cultured at 37°C and 5% CO₂ in Dulbecco's modified Eagle's medium (DMEM; Gibco) supplemented with 10% heat-inactivated fetal bovine serum (FBS; Atlanta Biologicals), L-glutamine (2mM; Gibco), streptomycin (100ug/mL; Gibco), and penicillin (100 U/mL; Gibco).

Viruses, Mutagenesis, and Infection

A full-length cDNA clone of 181/25 (CHIKV vaccine strain, a kind gift from Naomi Forrester, UT Medical Branch at Galveston, TX) was used to transcribe viral RNA using mMESSAGE mMACHINE SP6 Kit (Invitrogen). Viral RNA was transfected into BHK21 cells using Lipofectamine 2000 (Invitrogen) to rescue virus (89). Point mutations in the nsP3 gene were introduced into the 181/25 cDNA clone using the Quikchange Site-Directed Mutagenesis kit to create two viable nsP3^{MD} mutant viruses, G32S and Y114A (72). Virus stocks were grown in BHK-21 cells, and viral RNAs from stock virus were sequenced to confirm the mutation within the nsP3 gene. Virus titers were determined by plaque assay in Vero cells. C8-D1A cells were infected at the indicated multiplicity of infection (MOI) with CHIKV 181/25 (WT) and nsP3^{MD} mutants, G32S and Y114A. Cell viability was determined by trypan blue exclusion and reported as percent of day 0 cells.

Infectious Virus Titers by Plaque Assay

90% confluent 6-well plates of Vero cells were used for plaque assays. 10 fold dilutions of samples were made and 200 µL were added to each well and incubated at

37°C and 5% CO₂ for one hour with gentle shaking every 15 minutes. After an hour, each well was overlaid with 1.5 ml of 0.6% Bacto agar (BD) in modified Eagle medium (MEM; Gibco) The plates were incubated at 37°C, 5% CO₂ for 48 hours. The cells were then fixed with 10% formaldehyde in PBS and stained with 0.02% crystal violet for 30 minutes, and plaques were counted.

Infectious Center Assay with RNA and Virus

C8-D1A cells were infected with WT or nsP3^{MD} mutants at MOIs of 0.5 and 5 and incubated for 1 hour at 4°C and transferred to 37°C for 4h or were transfected with 10 µg of RNA from a full-length clone of CHIKV 181/25 (WT) or nsP3^{MD} mutants using the Amaxa nucleofector (73). Transfected and infected C8-D1A cells were trypsinized, and serial 10-fold dilutions of cells were plated on 90% confluent BHK-21 cells (for transfected cells) or Vero cells (for infected cells). After the addition of infected or transfected C8-D1A cells, cells were overlaid with 1.5ml of 0.6% Bacto agar in MEM. Plates were incubated for 48 hours at 37°C incubator and then were fixed with 10% formaldehyde in PBS and stained with 0.02% crystal violet, and plaques were counted.

Flow Cytometry for dsRNA staining

C8-D1A cells were infected with WT or nsP3^{MD} mutants, G32S and Y114A at an MOI of 5 or mock-infected and incubated at 37°C for the designated amounts of time. The cells were trypsinized followed by live/dead staining (Invitrogen) for 30 mins on ice in the dark. Cells were then fixed with 2% formaldehyde in PBS for 30 mins and were permeabilized with 0.2% Triton in FACS buffer (PBS with 0.4% 0.5mM EDTA and 0.5% BSA) for 30 minutes in ice. Cells were stained for dsRNA with J2 mouse monoclonal antibody (Mab) (1:1000 dilution; Scicons) and incubated for an hour on ice (73) followed

by secondary PE-conjugated anti-mouse IgG antibody (1:400 dilution) for 45 mins (73). Cells were analyzed on a FACS Canto flow cytometer (Becton-Dickinson). Histograms were plotted and percent of live cells positive for dsRNA was quantitated.

qRT PCR for PARP Gene Expression

C8-D1A cells either mock-infected or infected with CHIKV WT at MOI of 5 were harvested using the RLT buffer (Qiagen), and RNA was isolated using RNeasy Mini kit (Qiagen). cDNA was synthesized from RNA using the High Capacity cDNA reverse transcription kit (Life Technologies), and *Parp1*, *Parp9*, *Parp10*, *Parp12*, *Parp13*, and *Parp14* mRNAs were measured through qRT-PCR using TaqMan gene expression assays. Relative gene expression was determined using the $\Delta\Delta CT$ method using 0-hour control samples, and *Gapdh* for normalizing the PARP expression. Under the following conditions with 40 cycles: 2 minutes of 50°C, 10 minutes of 95°C, and 1 min of 60°C, PCR was performed in Applied Biosystems 7500 Real-time PCR machine (73).

qRT PCR for Viral RNA Synthesis

RNeasy Plus mini kit (Qiagen) was used to isolate total RNA from C8-D1A cells infected with CHIKV 181/25 or nsP3^{MD} mutants, G32S and Y114A at an MOI of 5. cDNA was synthesized from RNA using the High Capacity cDNA reverse transcription kit (Life Technologies) (73). qRT-PCR was performed using TaqMan primers and probes specific for the genomic (nsP2) and genomic plus sub-genomic (E2) regions of the CHIKV genome: for the CHIKV E2 gene: E2 922F 5'-GAAGAGTGGGTGACGCATAAG-3'; E2 1011R 5'-TGGATAACTGCGGCCAATAC-3'); for the TaqMan probe: CHK E2 949 5'-6-carboxyfluorescein [FAM]-ATCAGGTTAACCGTGCCGACTGAA-Minor groove binder (MGB) nonfluorescent quencher (NFQ)-3' (Applied Biosystems); for the CHIKV nsP2

gene: nsP2 1247F 5'-GTACGGAAGGTAAACTGGTATGG-3'; nsP2 1359R 5'-TCCACCTCCCCTCCTTAAT-3'); and for the TaqMan probe: CHIKV nsP2 1304 5'-(FAM)-TGCAGAACCCACCGAAAGGAACT-(MGB NFQ)-3' (Applied Biosystems) (73). Copies of viral RNA were quantified using a standard curve constructed from 10-fold dilutions of a pCRII-TOPO plasmid containing the CHIKV E2 or nsP2 region cDNA and normalized to endogenous rodent *Gapdh*. Data are plotted as mean CHIKV RNA copies per 10⁶ copies of *Gapdh* (73).

Western Blot Analysis of ADP Ribosylation and Protein Expression

C8-D1A cells were infected with WT or nsP3^{MD} mutants, G32S and Y114A at an MOI of 5 or mock-infected and incubated at 37°C for different time points. At each time point, cells were lysed in radioimmunoprecipitation assay (RIPA) buffer (50 mM Tris (pH 8), 1 % Triton X-100, 0.1 % of SDS, 150 mM NaCl, 1 mM EDTA, and 0.5 % Na₃VO₄·2H₂O) supplemented with protease and phosphatase inhibitors (Sigma) (73). The lysates for ADP-ribosylated protein analyses were collected in RIPA buffer supplemented with PARP inhibitor (Sigma) and PARP glycohydrolase inhibitor (Millipore) in addition to protease and phosphatase inhibitors. The lysates were incubated in ice for 30 minutes followed by centrifugation at 15,200 x g for 10 min to collect supernatant proteins. Dc protein assay (Bio-Rad) was performed to estimate total protein levels of lysates with BSA as the standard. 15 µg of proteins were loaded to 10% polyacrylamide gels, separated via electrophoresis, and transferred to nitrocellulose membranes. Membranes were blocked with 5% skim milk in PBS followed by incubating overnight at 4°C with polyclonal rabbit antibodies to CHIKV nsP1, nsP2, nsP3 (1:10000) (73,90), mouse Mab E2 structural proteins (1:1000) (CHK-187 11A4. F1.F4) (53), phosphor-eIF2 α , eIF2 α (1:1000; Cell

Signaling Technologies (CST)), pan ADPr-binding reagent (1:1000; Millipore), or β actin (1:5000; Millipore) diluted in 5% BSA in tris-buffered saline and Tween 20 (TBST). Secondary antibodies were HRP-conjugated either anti-mouse or anti-rabbit antibodies (1:1000; Cell Signaling Technologies) diluted in 2% milk and incubated for an hour at RT. Amersham ECL Prime Western Blotting Detection Reagent (GE Healthcare) was used to develop the membrane. ImageJ software from NIH was performed to analyze the densitometry of immunoblots from three to five independent experiments.

Puromycin translation assay

C8-D1A cells were infected with WT or nsP3^{MD} mutants, G32S and Y114A at an MOI of 5 or mock-infected and incubated at 37°C for different time points. After an hour of infection, fresh DMEM with 1% FBS was substituted. At particular time points, the media from the wells were removed, and DMEM containing 5 μ g/mL puromycin dihydrochloride (Sigma) was added and incubated for 10 minutes. The cells were then collected in RIPA buffer and immunoblotted using mouse anti-puromycin Mab clone 12D10 (1:1000; Millipore) (73). Membranes were incubated in secondary antibody HRP-conjugated anti-mouse IgG (1:10000; CST) and developed using Amersham ECL Prime Western Blotting Detection Reagent. ImageJ software from NIH was performed to analyze the densitometry of immunoblots from three independent experiments.

H₂O₂ Treatment

C8-D1A cells were mock-treated or treated with 2ml of DMEM containing 4 μ l of H₂O₂ (3 or 30%). After 15 mins of incubation, treated C8-D1A cells were washed once with PBS and collected in RIPA buffer for immunoblotting using pan ADPr-binding reagent

(1:1000; Millipore), followed by HRP-conjugated anti-rabbit IgG. The membrane was developed using the Amersham ECL Prime Western Blotting Detection Reagent.

³⁵S Pulse Chase Analysis of E2 Viral Protein Processing

C8-D1A cells were infected with WT or nsP3^{MD} mutants, G32S and Y114A at an MOI of 5 and incubated at 37°C for different time points. At 12- and 24-hour after infection, cells were washed with PBS followed by incubation in DMEM media without methionine (Met) and cysteine (Cys) (Gibco) for an hour. The cells were then pulsed with Met/Cys-free DMEM containing ³⁵S (100µCi/ml) for 30 minutes at 37°C, 5% CO₂. To chase the labeled proteins, cells were washed and incubated with media having 15mg/L of L-methionine for 0, 40, and 90 minutes. The supernatant fluids were collected in a 15ml conical tube and the cell lysates were collected in RIPA buffer containing phosphatase and protease inhibitors.

For immunoprecipitation, the DC assay was used to estimate protein amounts. 300 to 400 µg of total protein were incubated with 10 µg of mouse anti-E2 Mab at 4°C overnight with gentle rocking. 40 µl of prewashed ImmunoPure Immobilized Protein A/G (Pierce) beads were added to the mixture of cell lysate and E2 antibody, followed by overnight incubation at 4°C with gentle rocking. Beads were washed four times with RIPA buffer, and bound proteins were eluted by boiling with SDS loading buffer.

For supernatant fluids, 1/4th volume of polyethylene glycol solution (PEG 8000 and NaCl, pH 7.2) was added to the supernatant and incubated overnight at 4°C. Supernatants were centrifuged at 13,500 x g for 30 minutes to pellet the PEG precipitated virions. The pellet was boiled in SDS loading buffer. Eluted lysates and PEG-precipitated virions from supernatant samples were loaded onto 10% polyacrylamide gels and

electrophoresed. Gels were fixed with the fixing solution (10% acetic acid and 20% methanol) for 30 minutes and washed with water for an hour with water replacement every 15 minutes. Gels were enhanced with 1M sodium salicylate (Sigma) solution (pH 5 to 7) for 30 minutes and dried using a dryer at 56°C until the gel is dried. The radioactive gel was exposed to ECL X-ray (GE Healthcare) film until signals were detected.

IFN α and IFN β Enzyme ELISA

Supernatants of C8-D1A cells either mock-infected or infected with CHIKV 181/25 or nsP3^{MD} mutants, G32S and Y114A at an MOI of 5 were collected at different time points. The levels of IFN α and IFN β were measured using VeriKine ELISA kits (PBL Assay Science) according to the manufacturer's instructions (73). Assay ranges were 12.5-500 pg/mL for IFN α and 15.6-1000 pg/mL for IFN β .

In vitro IFN blockade

C8-D1A cells were infected with WT or nsP3^{MD} mutants, G32S and Y114A at an MOI of 5 and incubated at 37°C in DMEM 1%FBS containing antibodies against IFN α alone or IFN β alone or IFN α and β together or the Pan isotype control at concentrations of 10 μ g, 5 μ g, 1 μ g or nil (Leinco Technologies) and incubated for 8 or 24 hours. The cells were collected in RIPA buffer containing protease and phosphatase inhibitors and immunoblotted for phospho-STAT1 (1:500; CST), STAT1 (1:1000; CST), or β actin to observe STAT1 activation. Secondary anti rabbit or anti mouse antibodies were used, and the membrane was developed using Amersham ECL Prime Western Blotting Detection Reagent.

After optimizing the concentration of antibody for blocking IFN activity C8-D1A cells were infected with CHIKV WT and Y114A at an MOI of 5 and with G32S at an MOI of 0.5

and incubated at 37°C in DMEM 1%FBS with antibodies against IFN α and β together at concentrations of 10 μ g, 1 μ g or nil for different times. Supernatant was collected at each time point, and plaque assays were performed to measure the viral production.

Statistical Analysis

Prism 8 (GraphPad) was used for two-way ANOVA tests to calculate significant differences between different infections at a single time point. All results were shown as means \pm SD from three to five independent experiments.

2.3 Results

CHIKV with nsP3^{MD} Mutations That Affect ADPr- Binding and Hydrolase Activities Replicate Less Efficiently in Astrocytic Cells.

To determine the role of ADPr binding and hydrolase activities in viral replication in astrocytes, C8-D1A cells were infected with CHIKV 181/25 (WT) and nsP3^{MD} mutants G32S (decreased hydrolase and binding activities) and Y114A (decreased hydrolase and increased binding activities) at an MOI 5 (72,73). Virus production was quantitated by plaque formation in Vero cells (Fig. 2.1B), and cell viability was determined by trypan blue exclusion (Fig. 2.1A) WT and Y114A replicated with similar kinetics and at 24hpi Y114A had more viable cells ($P < 0.05$ vs WT) and higher viral titer than WT ($P < 0.01$ vs WT). The G32S virus replicated less well than WT and Y114A from 6hpi onwards ($P < 0.0001$ vs WT, $P < 0.05$ vs Y114A, 6hpi) except 24hpi and was also lower at 36hpi ($P < 0.0001$ vs WT/Y114A). The cell numbers at 36hpi in all three infected groups were similar.

nsP3^{MD} Mutations That Affect ADPr-Binding and Hydrolase Activities Affect the Formation of Functional Replication Complexes in Astrocytes.

The formation of functional replication complexes to amplify genomic viral RNA is determined by how successfully the replication complexes are established. To determine whether the activities of nsP3^{MD} affect the initiation of infection, infectious center assays were performed both by electroporating the same amount of RNA (Fig. 2.2A) and by infecting with virus at an MOI of 0.5 and 5 (Fig. 2.2B). RNA transcribed from WT and two nsP3^{MD} cDNA clones was electroporated into C8-D1A cells, co-cultured with BHK-21 cells and plaque formation assessed. G32S transfected C8-D1A cells produced fewer infectious centers than WT ($P < 0.0001$) and Y114A ($P < 0.01$). Y114A RNA transfected

C8-D1A cells also produced fewer infectious centers than WT ($P < 0.001$). Similar results were obtained when the infectious center assay was performed by exposing the cells to virus and mutants at the MOIs of 5 and 0.5. G32S mutant successfully infected fewer C8-D1A cells than WT at both MOIs (1267 G32S vs. 2592 WT infectious centers per 3×10^5 at an MOI of 0.5, $P < 0.0001$); (67667 G32S vs. 162500 WT infectious centers per 3×10^5 cells at an MOI of 5, $P < 0.0001$). However, Y114A mutant produced numbers of infectious centers similar to WT and more than G32S (1267 G32S vs. 2742 Y114A infectious centers per 3×10^5 cells at an MOI of 0.5, $P < 0.0001$); (67667 G32S vs. 145000 Y114A infectious centers per 3×10^5 at an MOI of 5, $P < 0.0001$). Therefore, ADPr-binding activity is more important than hydrolase activity for establishing infection.

After replication complexes are established, they are amplified with increasing numbers of spherules with dsRNA producing negative-strand template genomic RNA and positive strand genomic and subgenomic RNA. To assess amplification of replication complexes, C8-D1A cells were infected with WT and nsP3^{MD} mutants at an MOI of 5, stained with antibody to dsRNA and analyzed by flow cytometry (Fig. 2.3). At 4 and 6hpi, C8-D1A cells infected with WT and mutants did not show any difference in the number of dsRNA positive cells. However, at 8 and 12hpi, more C8-D1A cells infected with Y114A were positive for dsRNA than cells infected with WT and G32S (Fig. 2.3A and Fig. 2.3B). Individual C8-D1A cells infected with WT amplified more replication complexes than cells infected with G32S throughout the infection and cells infected with Y114A until 12hpi by comparing the fluorescent intensities (Figure 2.3C). Therefore, the nsP3^{MD} mutant virus with impaired ADP ribosyl hydrolase and binding activities made lesser replication

complexes compared to WT, while the mutant with better ADP ribosyl binding activity made replication complexes better or similar as compared to WT.

CHIKV Infection of C8-D1A Cells Induced increased PARP Gene Expression, But Not ADP-Ribosylation of Proteins.

In neuronal cells CHIKV infection leads to activation, but not increased *PARP* gene expression with increased ADP ribosylation of proteins. To determine whether there is modulation of PARP expression, C8-D1A cells were infected with CHIKV WT at an MOI of 5 and mRNAs quantified by qRT-PCR. PARPs known to be induced by IFN (*PARP* 9, 10, 12, 13 and 14) were induced with a peak at 6hpi ($P < 0.0001$) and sustained until 24hpi (Fig. 2.4A).

To determine whether CHIKV infection leads to ADP-ribosylation of proteins, lysates of C8-D1A cells infected with WT and nsP3^{MD} mutants were analyzed by immunoblot using an ADPr binding reagent that detects both MARs and PARs as well as antibody to the E2 glycoprotein (Fig. 2.4B and Fig. 2.4C). There was no or little ADP-ribosylation of proteins in CHIKV infected C8-D1A cells compared to mock-infected cells. Infection was confirmed by E2 protein expression (Fig. 2.4B). However, C8-D1A cells under oxidative stress after exposure to H₂O₂-containing media, induced ADP-ribosylation of proteins (Fig. 2.4D).

Viral RNA and Protein Synthesis and Processing in Infected Astrocytes

After spherules are formed for replication complexes at the plasma membrane, genomic and subgenomic RNAs are amplified within the infected cells. To assess viral RNA synthesis WT and nsP3^{MD} mutant infected cells, RNA was quantified by RT-qPCR (Fig. 2.5). Genomic viral RNA (Fig. 2.5B) made by the mutant with impaired ADP ribosyl

binding and hydrolase activity (G32S) is less throughout infection while subgenomic RNA (Fig. 2.5A) is less only early. The levels of Y114A mutant genomic and subgenomic RNA were similar to WT.

Nonstructural proteins translated from genomic RNA amplify replication complex formation. To determine how nsP3^{MD} mutation affects the translation of nsPs, C8-D1A cell lysates infected with CHIKV WT or nsP3^{MD} mutants at an MOI of 5 were immunoblotted to detect nsP synthesis (Fig. 2.6A). The G32S mutant produced less nsP early but reached levels of nsPs similar to WT and Y114A by 8hpi (Fig. 2.6B). As predicted by the dsRNA staining (Fig 2.3), Y114A mutant had greater nsP production throughout infection compared to WT and G32S. The increased binding ability of Y114A was associated with formation of more dsRNA-positive cells, more translation of nsPs and more genomic RNA.

Later stable replication complexes transcribe sgRNA for translation of structural proteins. To determine the synthesis of structural proteins, the lysates were immunoblotted to assess E2 glycoprotein production (Fig. 2.4A). Surprisingly, more E2 glycoprotein was made by cells infected with the G32S mutant than cells infected with WT and Y114A, especially at 24hpi ($P < 0.001$ vs WT, $P < 0.01$ vs Y114A) and 36 hpi ($P < 0.01$ vs WT) (Fig. 2.7A). Y114A mutant produced slightly more E2 protein than WT at 36hpi.

To determine whether the ADPr hydrolase and binding activities of nsP3^{MD} affects processing of the structural polyprotein in astrocytes was analyzed through a pulse-chase experiment. Infected cells were labeled for 30 min at 12 and 24h after infection, chased for the indicated times, and the E2 glycoprotein immunoprecipitated (Fig. 2.7B). At 12hpi

WT infected cells synthesized more pE2 than Y114A- infected cells, which produced more than G32S-infected cells. However, at 24hpi, the cells infected with nsP3^{MD} mutants G32S and Y114A had more pE2 than WT. However, the rate of synthesis was the same in all the three viruses. Virions released with labeled E2 were similar in amount at 12hpi whereas at 24hpi the nsP3^{MD} mutants especially G32S had more released E2. Therefore, mutant-infected cells produced more structural proteins and these proteins were processed normally.

Type I IFN Does Not Affect Virus Replication of nsP3^{MD} Mutants.

To determine the host response to virus infection, supernatants of C8-D1A cells infected with WT or nsP3^{MD} mutants were tested for type I IFN production by ELISA (Fig. 2.8). Y114A induced more astrocyte production of IFN β than WT ($P < 0.0001$ 6hpi; $P < 0.001$ 12hpi) and G32S ($P < 0.0001$) at early time points. Later in infection both nsP3^{MD} mutants induced more IFN α ($P < 0.05$) and IFN β ($P < 0.001$ G32S; $P < 0.01$ Y114A) than WT (Fig. 2.8A and Fig. 2.8B).

To determine whether type I IFN production actually improves WT or nsP3^{MD} mutant virus replication, IFN α and IFN β neutralizing antibodies were added to the cultures (Fig. 2.9 and Fig. 2.10). To optimize the concentration of antibodies for blocking IFN α and IFN β signaling in C8-D1A cells, CHIKV-infected C8-D1A cells were mock treated or treated with antibodies against IFN α , IFN β alone or in combination, or treated with isotype antibody at concentrations of 10 μ g, 5 μ g, and 1 μ g per ml. Activation of STAT1 was assessed by immunoblotting lysates for pSTAT1 (Fig 2.9). Although neither IFN α nor IFN β antibodies alone completely inhibited the activation of STAT1, IFN α and IFN β

antibodies in combination (10 μ g) blocked phosphorylation of STAT1 at 8 and 24hpi after infection (Fig. 2.9C and Fig. 2.9F).

The effect of blocking the type I IFN signaling on viral replication in C8-D1A cells infected with WT and Y114A at MOI of 5, and G32S infected cells at MOI of 0.5 was assessed by plaque assay (Fig. 2.10). There were no significant differences in virus production between antibody-treated and isotype-treated cells for WT and Y114A. Blocking by type I IFN antibody improved G32S replication compared to isotype treatment at an early time point (Fig. 2.10D, Fig. 2.10E, and Fig. 2.10F). While more type I IFN was produced upon the infection by nsP3^{MD} mutants, it had little effect on virus replication.

Impaired nsP3^{MD} ADP Ribosyl Binding and Hydrolase Activity Results in Decreased Host Translational Shutoff.

Alphaviruses induce host translational shutoff in part by activating PKR to phosphorylate translational initiation factor eIF2 α to facilitate translation of viral structural proteins from subgenomic RNA. We evaluated the effect of nsP3^{MD} mutations on host protein synthesis in astrocytes by immunoblotting for phospho eIF2 α (Fig. 2.11A and Fig. 2.11B) and by assessing overall protein synthesis by incorporation of puromycin, a structural analog of aminoacyl tRNA, into newly synthesized proteins (Fig. 2.11C and Fig. 2.11D). Phosphorylation of eIF2 α occurs very early (4hpi) in astrocytes as nsPs are translated and RNA is synthesized. At 6hpi, the ratio of phosphorylated eIF2 α relative to total eIF2 α was higher in WT-infected cells compared to G32S and Y114A-infected cells (P<0.05). At 24 hpi, however, Y114A had a higher p-eIF2 α : eIF2 α ratio than WT (P<0.01) or G32S (P<0.001). G32S had lower levels of p-eIF2 α throughout infection. The puromycin translational assay did not show any difference between WT and nsP3^{MD}

mutants until 24hpi. At 36hpi, there was less translational shut off in G32S-infected astrocytes than WT and Y114A infected cells.

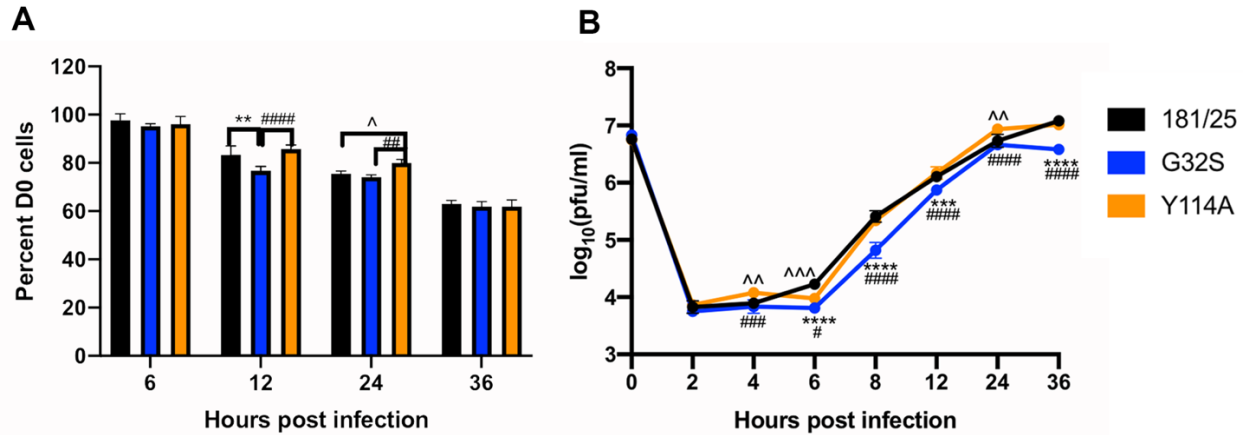


Figure 2.1 Astrocyte Cell Viability and Infectious Virus Production after Infection with CHIKV WT and nsP3^{MD} Mutants. C8-D1A cells were infected with 181/25 (WT) or two nsP3^{MD} mutants at an MOI of 5. (A) Cell viability was measured by trypan blue exclusion at four time points after infection. (B) Supernatant fluids were collected, serially diluted and plated on Vero cells for the plaque formation. The data represent the mean \pm SD from two independent experiments performed in triplicate. ** $P < 0.01$, *** $P < 0.001$, **** $P < 0.0001$ (WT vs. G32S); # $P < 0.05$, ## $P < 0.01$, ### $P < 0.001$, #### $P < 0.0001$ (G32S vs. Y114); ^ $P < 0.05$, ^^ $P < 0.01$, ^^[^] $P < 0.001$ (WT vs. Y114A).

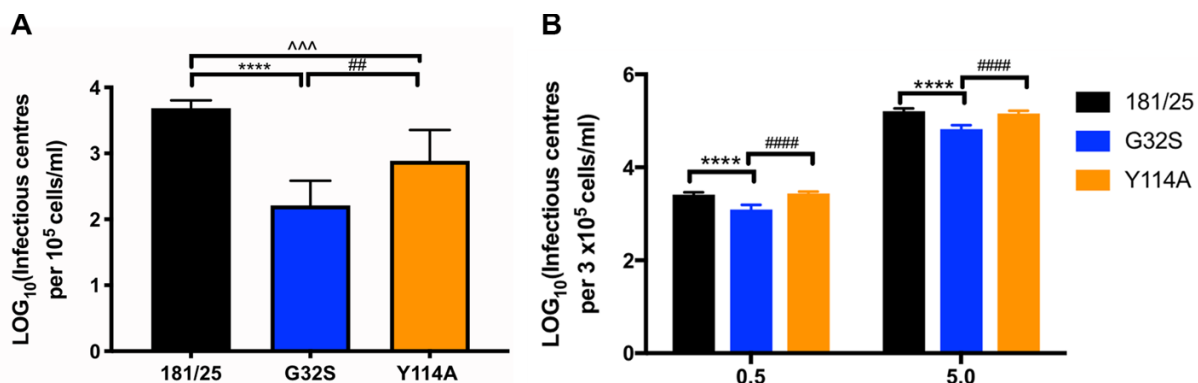


Figure 2.2: Establishment of Infection in Astrocytes by Transfected Viral RNA and Infectious Virus from WT and nsP3^{MD} mutants. (A) 10 μ g RNA of 181/25 (WT) or two nsP3^{MD} viral were electroporated into 10⁵ C8-D1A cells that were serially diluted and plated on confluent BHK21 cells, overlaid with agar and plaques produced by virus-infected cells counted. (B) C8-D1A cells were infected with WT or two nsP3^{MD} mutants at MOIs of 0.5 and 5, incubated an hour at 4^oC and 37^oC for 4 hours. Cells were trypsinized, serially diluted, plated on Vero cells, overlaid with agar and plaque formation assessed. The data indicate the mean \pm SD from two independent experiments done in triplicate. **** $P < 0.0001$ (WT vs. G32S); ## $P < 0.01$, #### $P < 0.0001$ (G32S vs. Y114); ^^[^] $P < 0.001$ (WT vs. Y114A).

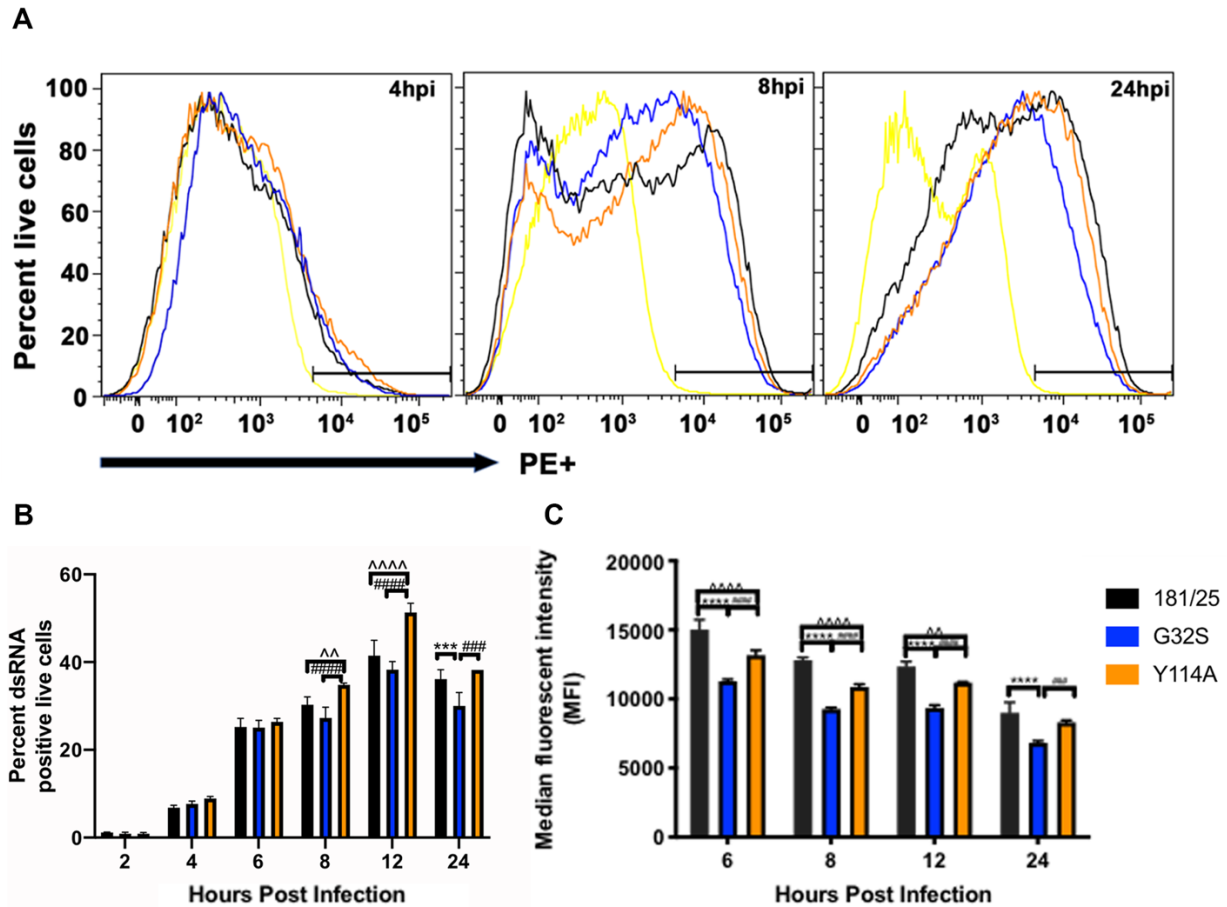


Figure 2.3 Formation and Amplification of Replication Complexes in Astrocytes Infected with WT and nsP3^{MD} Mutants. C8-D1A cells infected with 181/25 (WT) virus or nsP3^{MD} mutants at an MOI of 5. Cells were live/dead stained, fixed, permeabilized, and stained for dsRNA with J2 MAbs and analyzed by flow cytometry. (A) Histograms of representative data from three independent experiments done in triplicates. Yellow line indicates uninfected cells. (B) The percent of dsRNA positive live cells was quantified. (C) The median fluorescent intensities were measured. The data present the mean \pm SD from three independent experiments. *** $P < 0.001$, **** $P < 0.0001$ (WT vs. G32S); ### $P < 0.001$, #### $P < 0.0001$ (G32S vs. Y114A); ^^ $P < 0.01$, ^^^ $P < 0.0001$ (WT vs. Y114A).

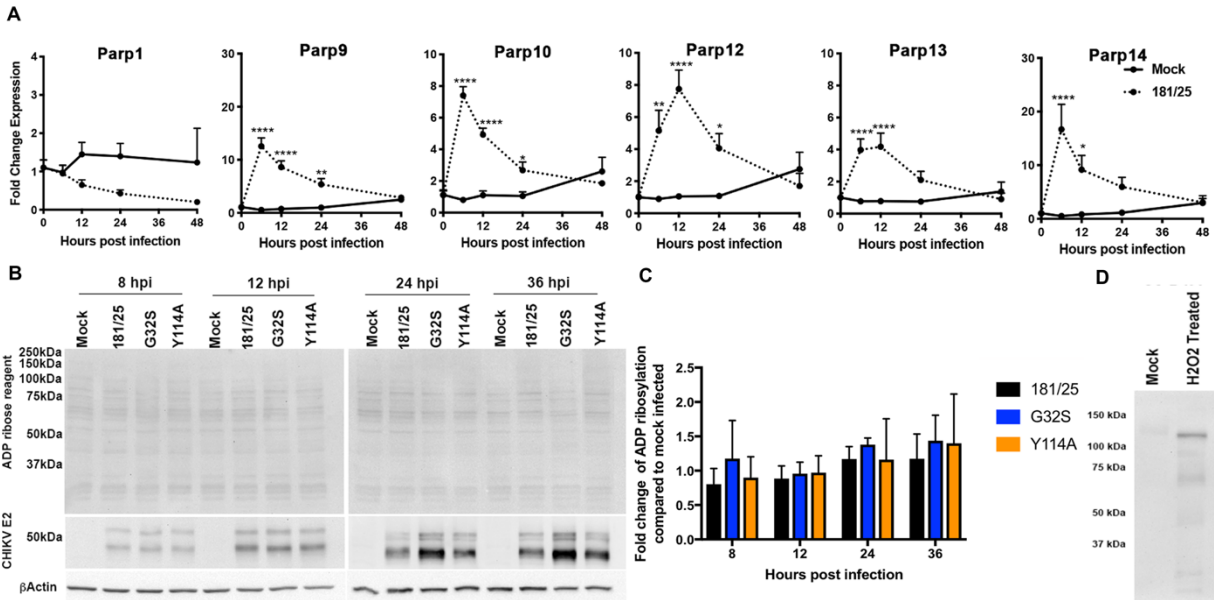


Figure 2.4 PARP mRNA Expression and ADP Ribosylation of Proteins During CHIKV WT and nsP3^{MD} Mutants Infection in Astrocytes. (A) C8-D1A cells infected with WT at an MOI of 5, and six different PARPs mRNAs were quantified by qRT-PCR. PARP mRNA change is indicated as the average \pm SD from three independent experiments. * $P < 0.05$, ** $P < 0.01$, **** $P < 0.0001$ (WT vs. Mock). (B) Lysates from C8-D1A cells infected with CHIKV 181/25 (WT) or two nsP3^{MD} mutants at an MOI of 5 were immunoblotted for ADPr and the E2 structural protein. β -actin was the loading control. A representative blot from three independent experiments is shown. (C) Quantification of ADPr was measured and normalized to actin level by densitometry from three independent experiments. (D) C8-D1A cell lysates treated with H₂O₂ and mock-treated lysates immunoblotted for ADPr. A representative blot from three independent experiments is shown.

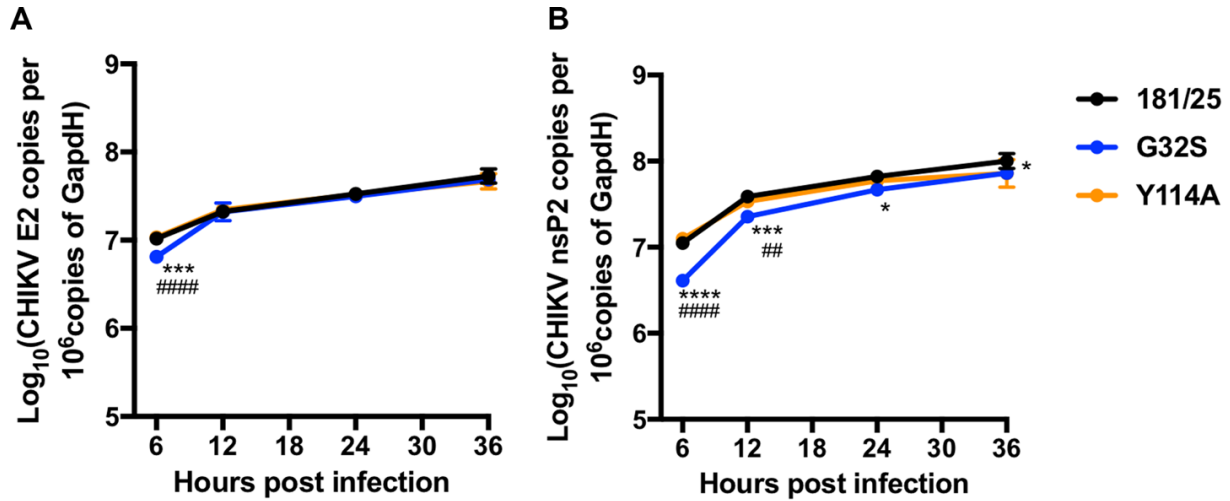


Figure 2.5 Levels of Genomic and Genomic Plus Subgenomic Viral RNA produced by Astrocytes infected with CHIKV WT and nsP3^{MD} Mutants. (A) Genomic and (B) genomic plus subgenomic RNA produced in C8-D1A cells infected with 181/25 (WT) virus or nsP3^{MD} mutants at an MOI of 5 were quantified by qRT-PCR. The mean \pm SD from three independent experiments are plotted. * $P < 0.05$, *** $P < 0.001$, **** $P < 0.0001$ (WT vs. G32S); ## $P < 0.01$, ##### $P < 0.0001$ (G32S vs. Y114)

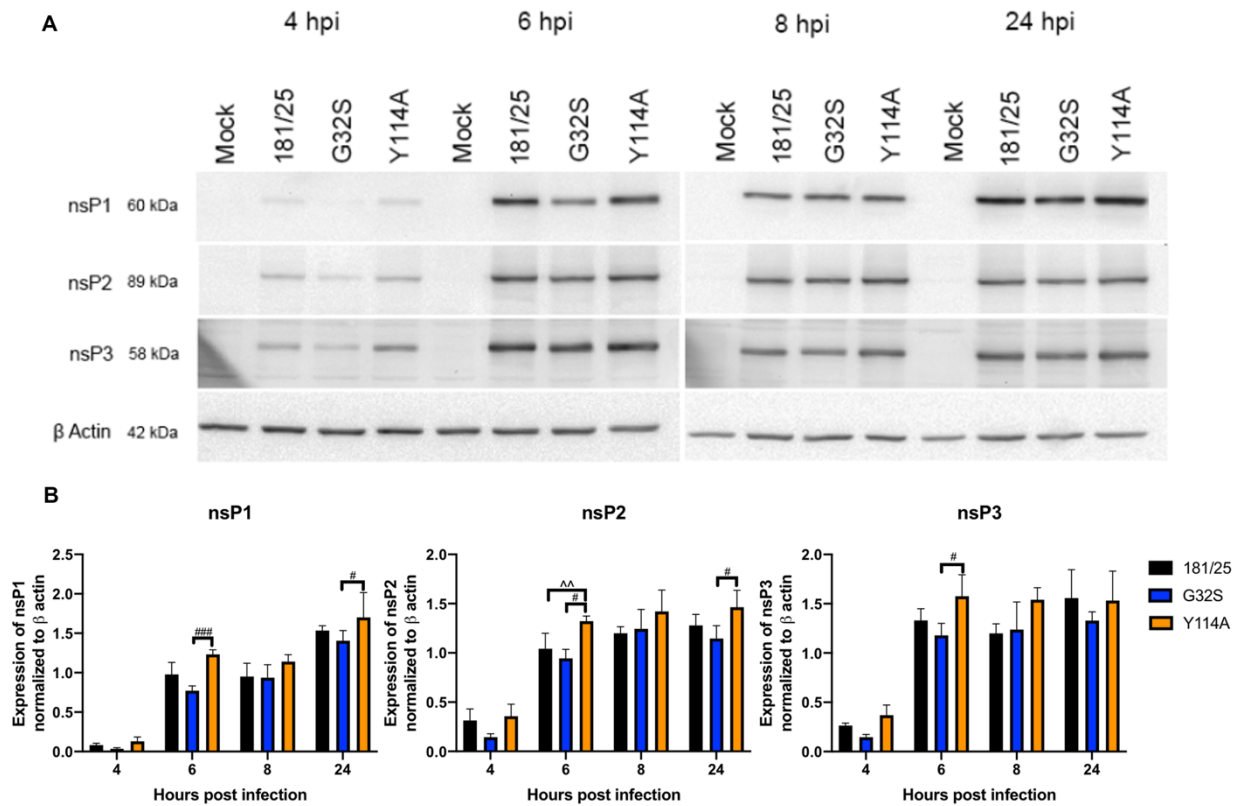


Figure 2.6 nsP Translation upon Infection by CHIKV WT and nsP3^{MD} Mutants in Astrocytes. Lysates from C8-D1A cells infected with CHIKV 181/25 (WT) or nsP3^{MD} mutants at an MOI of 5 were immunoblotted with antibodies against nsP1, nsP2, nsP3 and β -actin. (A) A representative image from five independent experiments. (B) Levels of nsPs measured by densitometry and normalized to actin levels graphed from five independent experiments. Data illustrate the mean \pm SD. # $P < 0.05$, ### $P < 0.001$ (G32S vs. Y114A); ^^ $P < 0.01$ (WT vs. Y114A).

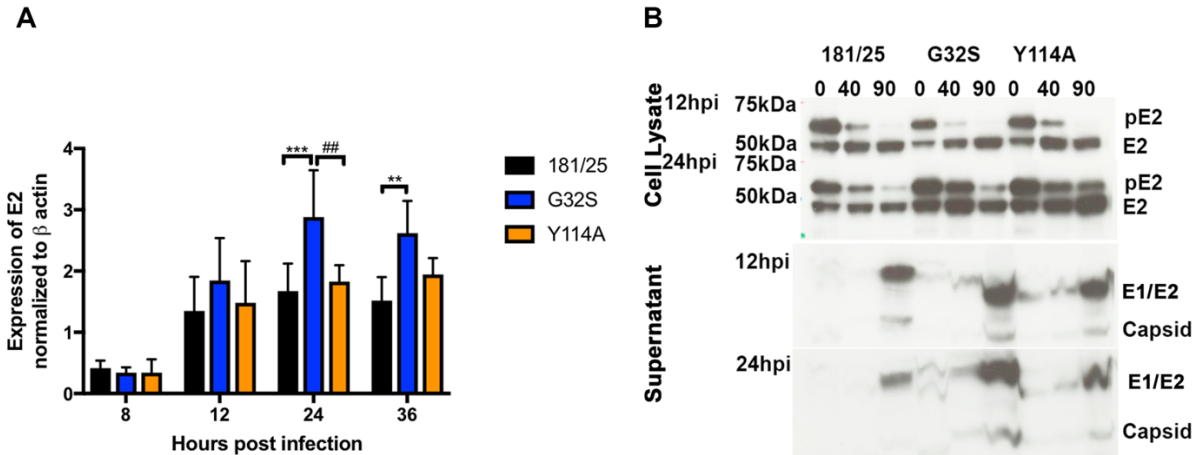


Figure 2.7 Effects of nsP3^{MD} Mutation on Viral Structural Protein Synthesis and Processing in Astrocytes. (A) Lysates from C8-D1A cells infected with CHIKV 181/25 (WT) or nsP3^{MD} mutants at an MOI of 5 were immunoblotted with antibodies to the E2 structural protein and β -actin (Fig 2.4B). Levels of E2 were normalized to actin by densitometry from three independent experiments and data graphed as the mean \pm SD. (B) Pulse-chase analysis of E2 processing in C8-D1A cells infected with WT or two mutants. Cells were pulsed with ³⁵S-methionine at 12 and 24h and immunoprecipitated with antibody to E2. Virions were PEG precipitated from supernatant fluids. The samples were subjected to polyacrylamide gel electrophoresis, fixed, dried, exposed to X-ray film and developed. The figure is representative of four independent experiments. ** $P < 0.01$, *** $P < 0.001$ (WT vs. G32S); ## $P < 0.01$ (G32S vs. Y114).

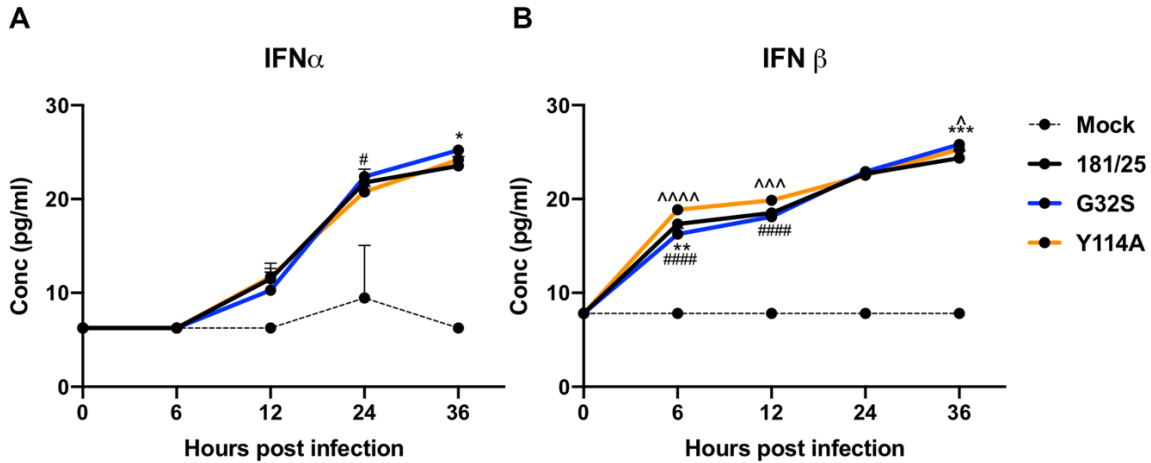


Figure 2.8 Type I IFN Production after CHIKV WT and nsP3^{MD} Mutants Infection of Astrocytes. (A and B) Amounts of type I IFN in supernatant fluids of C8-D1A cells infected with CHIKV 181/25 (WT) and nsP3^{MD} mutants were measured by ELISA. Data show the mean \pm SD from three independent experiments. * $P < 0.05$, ** $P < 0.01$, *** $P < 0.001$ (WT vs. G32S); # $P < 0.05$, ##### $P < 0.0001$ (G32S vs. Y114); ^ $P < 0.05$, ^^^ $P < 0.001$, ^^^^ $P < 0.0001$ (WT vs. Y114A).

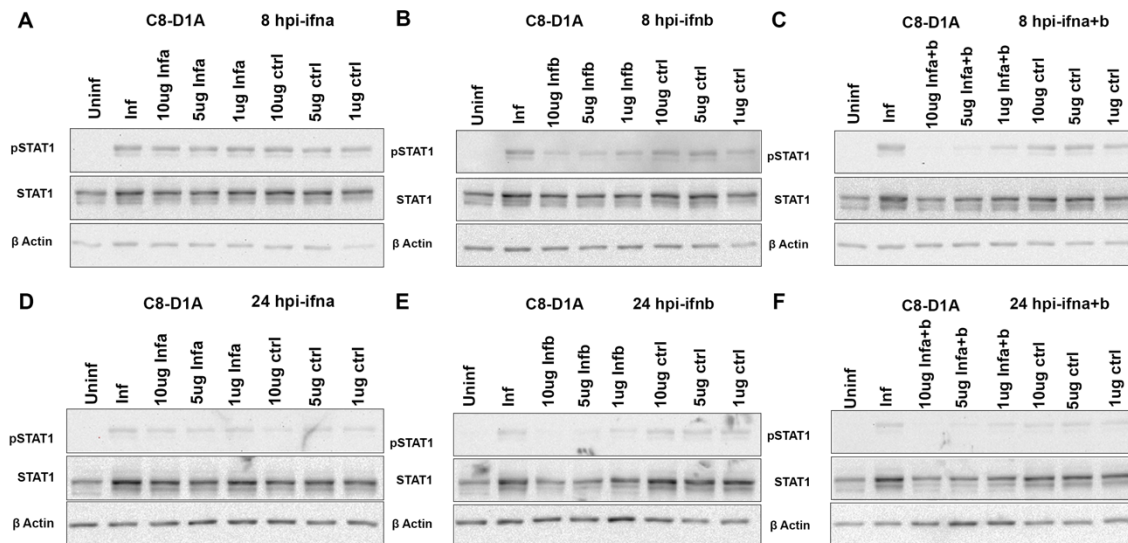


Figure 2.9 Optimization of Antibody Concentrations Required for Blocking of type I IFN signaling in CHIKV-Infected C8-D1A Cells. (A to F) C8-D1A cells uninfected or infected with 181/25 (WT) virus at an MOI of 5 and mock treated or treated with antibodies against IFN α , IFN β , or IFN α plus IFN β , or treated with isotype antibody at 10 μ g, 5 μ g, and 1 μ g/ml. Lysates were immunoblotted with antibodies against phospho STAT 1, STAT 1, and β -actin at 8 and 24hpi.

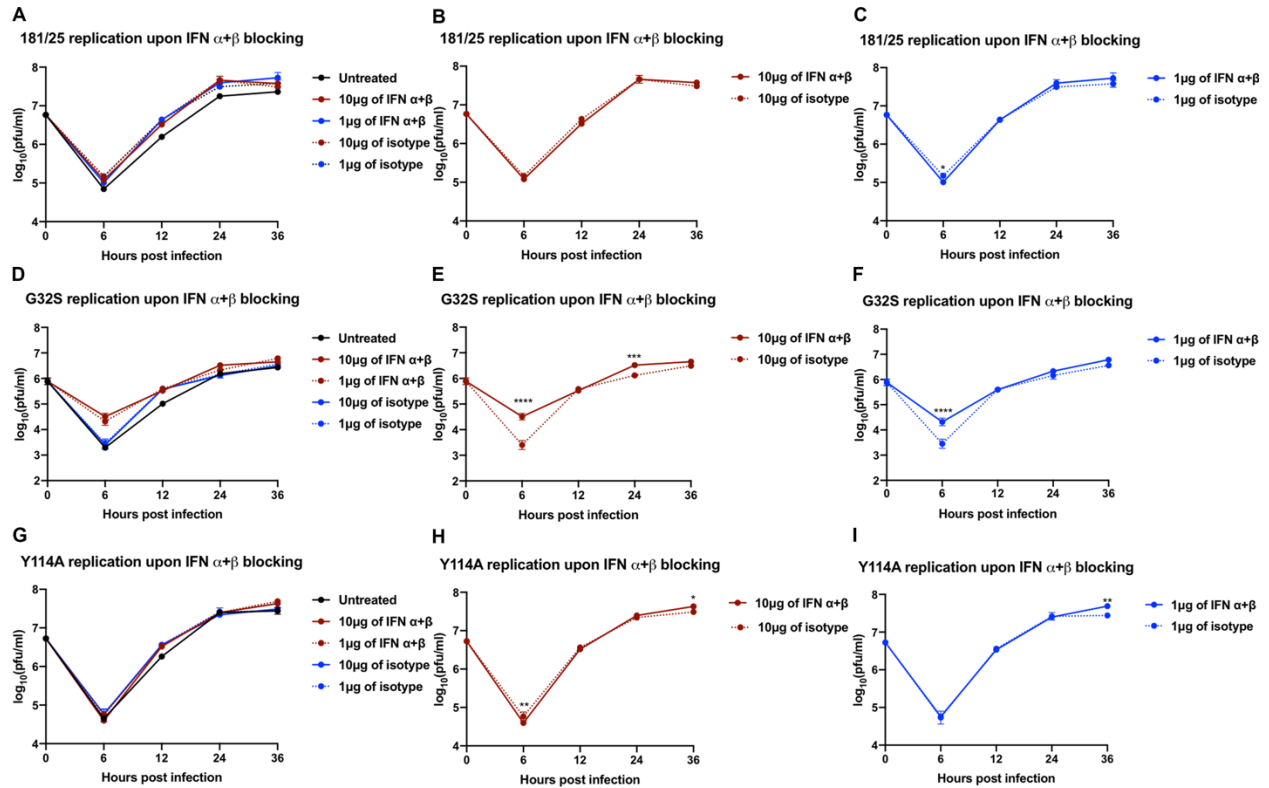


Figure 2.10 Infectious Virus Produced by CHIKV WT and nsP3^{MD} Mutants upon Type I IFN Blocking in Astrocytes. C8-D1A cells were infected with WT and Y114A at MOI of 5 and G32S at MOI of 0.5 and treated with either 10 μ g or 1 μ g of type I IFN blocking or isotype control antibodies. Serially diluted culture fluids were assessed for plaque formation on Vero cells. (A-C) WT replication in the presence of control and IFN α plus IFN β antibody at 1 (A,C) and 10 (A, C) μ g/ml. (D-F) G32S replication in the presence of control and IFN α plus IFN β antibody at 1 (D,F) and 10 (D,E) μ g/ml. (G-I) Y114A replication in the presence of control and IFN α plus IFN β antibody at 1 (G,I) and 10 (G,H) μ g/ml. Data are presented as mean \pm SD from three independent experiments. * $P < 0.05$, ** $P < 0.01$, *** $P < 0.001$, **** $P < 0.0001$ (Type I IFN blocking antibodies vs. isotype controls).

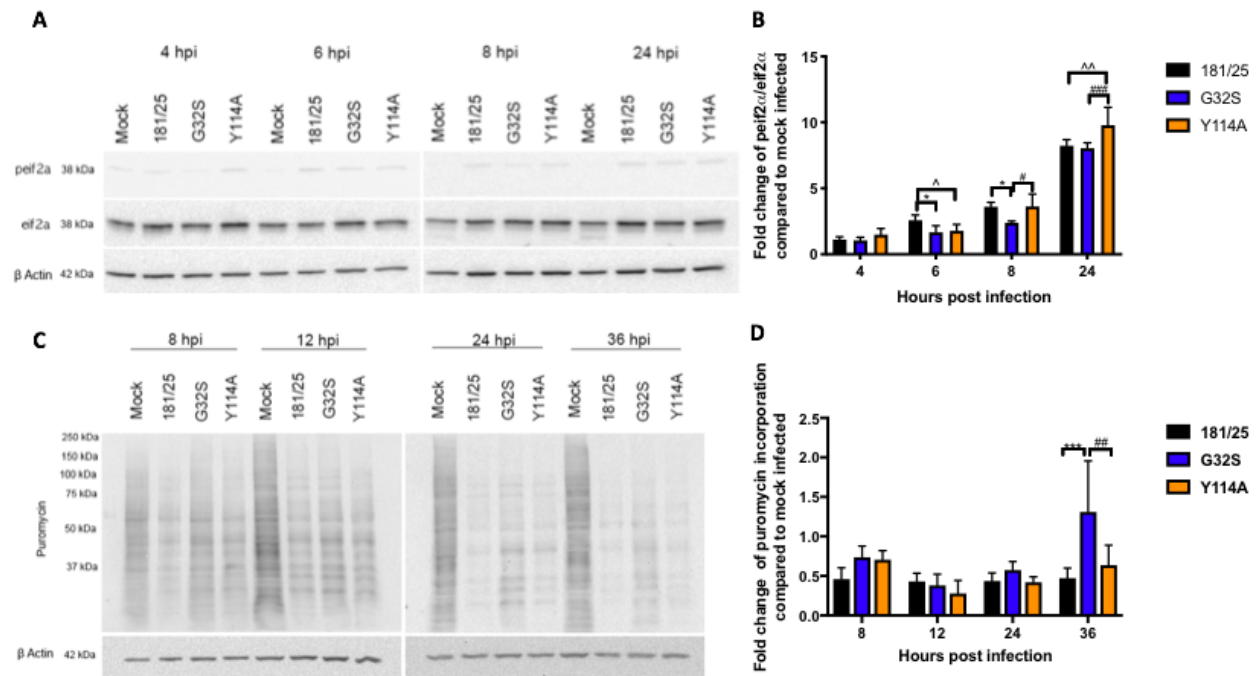


Figure 2.11 Host Translational Shut off in Astrocytes Infected with CHIKV WT and nsP3^{MD} Mutants. C8-D1A cells were infected with CHIKV 181/25 (WT) or nsP3^{MD} mutants at an MOI of 5 (A, B) Lysates were immunoblotted for phosphorylated eIF2 α , total eIF2 α , and β actin. (A) A representative blot from four different experiments. (B) The ratio of phosphorylated eIF2 α to total eIF2 α determined by densitometry and normalized to β actin. Data are plotted as the mean fold change relative to mock-infected C8-D1A cells \pm SD. (C, D) Lysates from infected C8-D1A cells incubated with medium containing puromycin were immunoblotted with antibodies to puromycin and β actin. (C) Representative image from three independent experiments. (D) Puromycin staining normalized to β actin plotted as mean fold change relative to mock-infected C8-D1A cells \pm SD. * $P < 0.05$, *** $P < 0.001$ (WT vs. G32S); # $P < 0.05$, ## $P < 0.01$, ### $P < 0.001$ (G32S vs. Y114A); ^ $P < 0.05$, ^^ $P < 0.01$ (WT vs. Y114A).

2.4 Discussion

Recent outbreaks of the reemerging Old-World alphavirus CHIKV demonstrate unusual neurovirulence among patients. When CHIKV crosses the blood brain barrier and cerebrospinal fluid, infection of CNS cells, such as neurons, astrocytes, and microglial cells can occur (26). Death of CNS cells induced by viral infection can lead to long-term neurological sequelae in patients when cells cannot be replaced (26). Alphavirus nsP3 influences virus replication in the brain and is an important determinant of neurovirulence (68, 72, 73, 74). The macrodomain of nsP3 has mono ADPr binding and hydrolase activities that affect formation of replication complexes and synthesis of viral RNA (72, 73). Mutations introduced into either the catalytic loop related to hydrolase activity or the pyrophosphate loop related to binding activity of the active site, attenuated neurovirulence for mice (73, 74, 75). Our previous studies to assess the role of the MD in viral replication analyzed neuronal infection, In this study, we analyzed infection of astrocytes, the most frequent target for CHIKV of the CNS.

The alphavirus virus replication cycle begins with translation of the nonstructural proteins, establishment and amplification of replication complexes for the synthesis of genomic and subgenomic RNA (Fig. 2.5), translation of viral structural proteins (Fig. 2.4 and Fig. 2.6), and production of infectious virus (Fig 2.1B). Virus with an nsP3^{MD} mutation that decreased binding and hydrolase activities (G32S) was inefficient at initiation of infection and formation of functional replication complexes (Fig. 2.2 and Fig. 2.3) compared to WT. G32S produced less genomic and subgenomic RNA, less nsP synthesis, and infectious virus with limited host translational shut off in infected astrocytes.

When binding activity is increased but hydrolase activity is decreased in nsP3^{MD} mutant Y114A, the initiation of infection and formation of replication complexes were not compromised at earlier time points and at later time points, Y114A produced more replication complexes, although genomic and subgenomic RNA, nsP synthesis, and infectious virus were similar to WT. Similar to what we observed in neuronal cells, increased ADPr binding activities partially compensated for decreased hydrolase activity and made the mutants produce more RNA, more nsP translation, and eventually the virus production. Thus, nsP3^{MD} binding and hydrolase activities are important in the virus replication cycle in astrocytes as well as neurons.

However, differences in the cellular responses were observed. C8-D1A cells produced type I IFN (Fig. 2.8), and upregulated the expression of IFN-stimulated PARP gene expression upon infection while neuronal cell did not (Fig. 2.4D). However, blocking IFN signaling with antibodies to both IFN α and IFN β did not alter virus replication (Fig. 2.9). Despite increased PARP gene expression, infection of astrocytic cells did not increase ADP ribosylation of proteins as was seen with neuronal cells. The results may be explained by production of more infectious virus after the first round of replication in astrocytes. Infected astrocytes produced 3 to 100 times more CHIKV than infected neurons (53 and Fig. 2.1B) and hydrolase activity of nsP3 might remove ADPribose moiety from MARylated substrates, with increased expression of PARPs.

Importantly, the defect in production of structural proteins associated with nsP3^{MD} mutants in neurons was not observed in astrocytes. NSC34 neuronal cells infected with nsP3^{MD} mutants showed defects in structural protein synthesis compared to WT. In contrast, astrocytes infected with nsP3^{MD} mutants produced more structural proteins than

WT (Fig. 2.7) and had similar processing rates (Fig. 2.7B). The reason for this is currently unclear and a topic for further investigation.

Chapter 3

Understanding the signaling pathways leading to the type I interferon production by astrocytes, but not neurons.

3.1 Introduction

Both the innate and adaptive immune systems are essential to protect the host from pathogens (51). The innate immune system is the frontline of the battle by enabling the host to sense the existence of the pathogen, inhibiting replication, and alerting the adaptive immune response for activation (47). Pattern Recognition Receptors (PRRs) recognize specific pathogen-associated molecular patterns and send signals to activate proteins and induce gene expression. The upregulation of antiviral genes induces production of antiviral proteins, inflammatory chemokines and cytokines to counter the pathogen. Natural Killer (NK) cells induce cytolysis of infected cells to eliminate existing pathogens (57). Dendritic cells and other antigen-presenting cells process the antigens and express the epitopes on MHC class I molecules and MHC Class II molecules to activate adaptive immune cells such as B cells and T cells.

The adaptive immune system can recognize processed foreign antigens, develop the response against specific antigens of the pathogens, and establish memory of the antigens to combat future infection (49). While MHC Class I molecules are expressed by all nucleated cells of vertebrates, MHC Class II is found mainly on the surface of antigen-presenting cells. B cells produce specific immunoglobulins against epitopes of viral proteins. Among the functions of antibodies are neutralization to block entry, opsonization to induce phagocytosis, and activation of complement. T cells trained through negative and positive selection against self-antigens in the thymus target virus-specific antigens

(49). Memory cells develop from active B cells and T cells in the lymph node to prepare against future infection. When a secondary infection happens, faster and stronger adaptive immune responses are triggered by memory cells.

Cells identify viruses using TLRs, RLRs, and NLRs as their main pattern recognition receptors (PRRs) (50). After recognition of ssRNA and dsRNA or viral proteins by the receptors, they trigger phosphorylation of downstream signaling molecules to activate the type I IFN and NF κ B response pathways (50). TLRs and NLRs recognize ssRNA and activate the TRAF6 for phosphorylation of IKK β and I κ B, releasing NF κ B to stimulate production of IL1 β and TNF α that induce inflammation at sites of infection (50). TLR3 and RLRs activate the TRAF3 pathway to phosphorylate IRF3/7 and induce production of IFN α and IFN β (48, 49). Type I IFN, cytokines, and interleukins can act through autocrine and paracrine signaling to activate the JAK/STAT pathway and upregulate expression of antiviral proteins. One ISG is the MHC class I molecule that presents processed viral peptides for presentation on the surface of infected cells. In addition, NK cells and inflammatory chemokines recruit and activate macrophages. NK cells also kill infected cells using perforin and secrete IFN γ and TNF α to induce MHC Class II molecules (57). MHC Class II molecules present viral peptides that activate CD4⁺ T cells, and MHC Class I molecules present viral peptides that activate CD8⁺ T cells. CD4⁺ T cells produce diverse interleukins to regulate the adaptive immune response, and CD8⁺ T cells lyse virus-infected cells. B cells secrete specific antibodies with the help of CD4⁺ T cells. While cell-mediated innate and adaptive immune responses can clear the virus and cause neurological disease by destroying infected host cells, PRR-induced innate responses are important for detection early and induction of type I IFN (58).

Compared to neuronal cells, dsRNA staining of CHIKV infected astrocytes demonstrated production of more replication complexes faster. Astrocytes also produced more copies of viral RNA, higher levels of nsPs and more infectious virus compared to neurons indicating greater susceptibility of astrocytes to CHIKV infection. Upon CHIKV infection, type I IFNs were produced by astrocytes, but not by neurons. There was increased expression of IFN-stimulated PARPs upon alphavirus infection in CNS tissues of mice and in astrocytes, whereas in neuronal cells PARP activation without increased mRNA expression during virus infection resulted in ADP-ribosylation of proteins. The present study was pursued to better understand the innate immune pathways that activate type I IFN in CHIKV-infected astrocytes, but not in neurons.

3.2 Materials and Methods

Cell Culture and IFN and Poly (I:C) Treatment

The murine astrocytic C8-D1A (astrocyte type I clone) cell line from American Type Culture Collection, murine neuronal NSC34 cell line (from Neil Cashman, University of British Columbia) (91), and African green monkey epithelial (Vero) cells were cultured at 37°C and 5% CO₂ in Dulbecco's modified Eagle's medium (DMEM; Gibco) supplemented with 10% heat-inactivated fetal bovine serum (FBS; Atlanta Biologicals), L-glutamine (2mM; Gibco), streptomycin (100µg/mL; Gibco), and penicillin (100U/mL; Gibco). To mimic dsRNA activation of innate responses during virus infection, C8-D1A and NSC34 cells were treated with low molecular weight (LMW) (1µg/ml) and high molecular weight (HMW) (1µg/ml; Invivogen) poly (I:C), combined with transfection reagent, LyoVec™ in DMEM. For IFN stimulation, cells were treated with 2µl of IFN α A/D (100U/ml, PBL Bioscience) in DMEM for different amounts of time.

Viruses and Infection

A full-length cDNA clone of 181/25 (a kind gift from Naomi Forrester, UT Medical Branch at Galveston, TX) was used to transcribe viral RNA using mMACHINE mMACHINE SP6 Kit (Invitrogen). For virus stocks BHK21 cells were transfected with viral RNA using Lipofectamine 2000 (Invitrogen) (89). Titers were determined by plaque assay in Vero cells. C8-D1A cells and NSC34 cells were infected at an MOI of 5 with CHIKV 181/25 (WT). Cell viability was measured by trypan blue exclusion and calculated as the percent of Day 0 cells.

Infectious Virus Titers by Plaque Assay

90% confluent 6-well plates of Vero cells were used for plaque assays. 200 μ L of serially 10-fold diluted culture fluids were added to the monolayer and incubated at 37°C and 5% CO₂ for an hour with gentle shaking every 15 minutes. After an hour, the cells were overlaid with 1.5 ml of 0.6% Bacto Agar (BD) in Modified Eagle Medium (MEM; Gibco). The plates were incubated at 37°C for 2 days. The cells were fixed with 10% formaldehyde in PBS and stained with 0.02% crystal violet for 30 minutes and plaques were counted (73).

IFN α and IFN β ELISA

Supernatants of C8-D1A cells infected with CHIKV 181/25 at an MOI of 5 were collected at 12 and 36hpi. The levels of IFN α and IFN β in the supernatants were measured using VeriKine ELISA kits (PBL Assay Science) according to the manufacturer's instructions.

qRT PCR for Type I IFN, TLRs, and RLRs

C8-D1A cells and NSC-34 cells either mock-infected or infected with CHIKV WT at an MOI of 5 were harvested in RLT buffer (Qiagen). Total RNA was isolated using the RNeasy Plus Mini Kit (Qiagen) and cDNA was synthesized using the High Capacity cDNA Reverse Transcription Kit (Life Technologies) (73). TaqMan gene expression arrays (Integrated DNA Technologies) were used to measure *IRF3*, *IRF7*, *IFN α* , *IFN β* , *RIG-I*, *MDA5*, *TLR3*, *TLR7*, *TLR 8*, *TLR9*, and *Myd88* mRNA levels. The PCR conditions were 40 cycles of 2 minutes at 50°C, 10 minutes at 95°C, and 1 min at 60°C performed in Applied Biosystems 7500 Real-time PCR machine (73). Relative gene expression was determined using the $\Delta\Delta$ Ct method using 0-hour control samples, and *Gapdh* and *RPS-29* were used for normalizing type I IFN, TLR, and RLR mRNA expression.

Western Blot Analysis of Protein Expression

C8-D1A and NSC34 cells were infected with WT at an MOI of 5 or mock-infected and incubated at 37°C for various times. At selected time points, the cells were lysed in RIPA buffer (50 mM Tris (pH 8), 1 % Triton X-100, 0.1 % of SDS, 150 mM NaCl, 1 mM EDTA, and 0.5 % Na₃VO₄·2H₂O) supplemented with protease and phosphatase inhibitors (Sigma) (73) on ice for 30 minutes followed by centrifuging 15,200 x g for 10 min to collect the supernatant containing proteins. The Dc protein assay (Bio-Rad) was performed to estimate total protein in lysates with BSA as the standard. 15 to 20 µg of protein were loaded onto a 10% polyacrylamide gel, separated via electrophoresis, and transferred to nitrocellulose membranes. The membranes were blocked with 5% skim milk in PBS at RT followed by incubating overnight at 4°C with polyclonal rabbit antibodies to CHIKV nsP1, nsP2, nsP3 (1:10000), nsP4 (1:200) (73,90), mouse MAb E2 structural proteins (1:1000; CHK-187 11A4. F1.F4) (73), RIG-I, MAVS, phospho-TBK1, TBK1, phospho-IRF3, IRF3, phospho-IRF7 (1:1000; Cell Signaling Technologies), MDA5, IRF7 (1:500; Abcam), TRAF3 (1:500; R&D Systems) or β actin (1:5000; Millipore) diluted in 5% BSA in TBST. Secondary antibodies were HRP-conjugated anti-mouse, anti-rabbit, or anti-rat IgG (1:1000; Cell Signaling Technologies) diluted in 2% milk and incubated for an hour at RT. Amersham ECL Prime Western Blotting Detection Reagent (GE Healthcare) was used to develop the membrane. ImageJ software from NIH was used to analyze the densitometry of immunoblots from three to five independent experiments.

Statistical Analysis

Prism 8 (GraphPad) was used for two-way ANOVA tests to calculate significant differences between different infections at a single time point. All results are shown as means \pm SD from three to five independent experiments.

3.3 Results

Compared to Neurons Astrocytes Produce More Infectious Viruses and Initiate Viral Protein Synthesis Earlier.

To assess differences in CHIKV replication between the astrocytes and neurons, the same number of neuronal NSC34 and astrocyte C8-D1A cells were infected with CHIKV 181/25 (WT) and virus production was measured using plaque assays (Fig. 3.1B) and cell viability was assessed using trypan blue exclusion (Fig. 3.1A). C8-D1A cells produced more infectious virus than NSC34 from 6hpi ($P < 0.001$) onwards. Peak virus production was at 24hpi with higher viral titers in C8-D1A cells ($P < 0.001$) but similar titers at 36hpi. Viability of C8-D1A cells was better at 6hpi ($P < 0.05$), 12hpi ($P < 0.001$), and 24hpi ($P < 0.01$) than NSC34 cells. At 36hpi both viability and titer were decreased ($P < 0.0001$).

To determine whether viral protein translation is affected by cell type, a similar number of NSC34 and C8-D1A cells were infected with WT CHIKV at an MOI of 5. Lysates were immunoblotted for nsP1, nsP2, nsP3, nsP4 and E2 glycoprotein (Fig. 3.2A). Infected C8-D1A cells produced detectable amounts of viral proteins by 6hpi (nsP1, $P < 0.01$); (nsP2, $P < 0.0001$); (nsP3, $P < 0.001$); (nsP4, $P < 0.001$); (E2, $P < 0.05$) while viral protein production by NSC34 cells was not detected until 12hpi. (Fig. 3.2B). At later time points, amounts of viral protein synthesized by astrocytes slightly, but not significantly, higher than neurons.

Phosphorylation of IRF3 Leads to More Type I IFN Production in Astrocytes.

To compare activation of the type I IFN response in neurons and astrocytes, a similar number of NSC34 and C8-D1A cells were infected with CHIKV at MOI 5 and the mRNA expression of several immune factors were determined by qRT-PCR. There was

no change in levels of *Ifn α* and *Ifn β* in neurons compared to mock-infected cells, whereas in astrocytes both *Ifn α* and *Ifn β* increased with peaks at 24hpi and 36hpi ($P < 0.0001$) (Fig. 3.3A and Fig. 3.3B). Levels of type I IFN protein produced by CHIKV-infected cells were determined by ELISA. IFN α was detectable by 12hpi and IFN β by 6hpi after infection of C8-D1A cells (adapted from Fig 2.8, Fig 3.3C) ($P < 0.0001$). However, type I IFN protein was not detectable at any time after infection of NSC34 cells (73).

IRF3 and IRF7 are the fundamental transcriptional regulators of the type I IFN response to viral infection. Expression of *Irf3* in neurons and astrocytes did not change after infection while *Irf7* increased from 12hpi onwards, as compared to mock-infected cells, only in astrocytes ($P < 0.0001$) (Fig. 3.3D and Fig. 3.3E). To assess activation of IRFs during infection, lysates from NSC34 and C8-D1A cells infected with WT CHIKV at an MOI of 5 were immunoblotted for phospho-IRF3, total IRF3, phospho-IRF7, and total IRF7 (Fig. 3.4). Phosphorylation of IRF7 was not detected until 24hpi and at 36hpi, C8-D1A cells had more phosphorylated IRF7 than NSC34 cells ($P < 0.0001$) (Fig. 3.4A and Fig. 3.4B). Phosphorylation of IRF3 gradually increased from 12hpi to 36hpi in astrocytes ($P < 0.0001$) but not in neurons (Fig. 3.4C and Fig. 3.4D). Although transcript levels of IRF7 increased, the type I IFN response in astrocytes is mainly regulated by activation of IRF3 .

RIG-I Like Receptor pathway is Activated in Astrocytes upon Poly (I:C) Treatment Leading to Phosphorylation of IRF7 but not in Neurons.

To determine the role of the RIG-I Like Receptor pathway in the induction of type I IFN production by astrocytes and not neurons, both cells were treated with either universal type I IFN A/D or the synthetic double-stranded RNA analog poly (I:C).

Expression of RLRs and their downstream mediators was tested by immunoblotting (Fig 3.5). When treated with low molecular weight (LMW) poly I:C (length between 0.2kb to 1kb) and high molecular weight (HMW) poly I:C (length between 1.5kb to 8kb) astrocytes increased expression of RIG-I and MDA5, phosphorylated TBK-1 and IRF7. MAVS and TRAF3 expression and phosphorylation of IRF3 was constitutive in C8-D1A cells. However, poly (I:C) treatment of neurons did not activate any components of the RLR signaling pathway, although MAVS and TRAF3 were constitutively expressed (Fig 3.5).

Treatment with universal type I IFN A/D increased expression of RIG-I in both cells while MDA5 activation was more pronounced in astrocytes than in neurons. Phosphorylation of IRF3 by treatment with universal type I IFN A/D was more pronounced in astrocytes than in neurons, whereas phosphorylation of IRF7 compared to mock-treated cells did not change in either cell line (Fig 3.5). Additional experiments are needed to identify why activation of IRF3 occurs in astrocytes but not in neurons.

RIG-I Like Receptor Pathway in Astrocytes is Activated Early upon Infection Compared to Neurons.

To determine which innate immune response is responsible for the phosphorylation of IRF3 and activation of type I IFN by CHIKV infection, C8-D1A and NSC34 cells were infected with WT CHIKV at an MOI of 5, and mRNA levels were measured by qRT-PCR and protein levels by immunoblots (Fig. 3.6A and B). *Rig-i* mRNA was increased in infected C8-D1A cells by 6hpi ($P < 0.0001$) and at 12hpi ($P < 0.01$), whereas in infected NSC34 cells an increase was not detectable until 36hpi ($P < 0.001$). *Mda5* mRNA was increased only in infected C8-D1A cells from 6hpi ($P < 0.0001$) through 24hpi ($P < 0.0001$). RIG-I receptor protein increased in CHIKV infected astrocytes

compared to the mock but in neurons this was observed only at 24hpi (Fig. 3.6C and Fig. 3.6D). The activation of the adaptor protein MAVS with appearance of a 52kDa cleavage product from the parent 75kDa at 24hpi and 36hpi was apparent in astrocytes, but not in neurons. There was less phosphoTBK-1 in infected astrocytes at 24hpi and 36hpi compared to mock-infected cells (Fig. 3.6C).

Toll-Like Receptor Pathway upon Infection in Astrocytes.

To determine whether the toll-like receptor pathway is involved in innate immune response upon CHIKV infection in astrocytes and neurons, C8D-1A and NSC34 cells were infected at an MOI of 5 and mRNA levels of *Tlr3*, *Tlr7*, *Tlr9*, and *Myd88* were measured by qRT-PCR. (Fig. 3.7). Expression of *Tlr3* ($P < 0.01$) and *Myd88* ($P < 0.0001$) in astrocytes peaked at 6 hpi, but not in neurons. Expression of *Tlr7* and *Tlr9* was not modulated in either cell line by infection. More experiments must be done to understand the role of the TLR pathway in CHIKV infection in astrocytes and neurons.

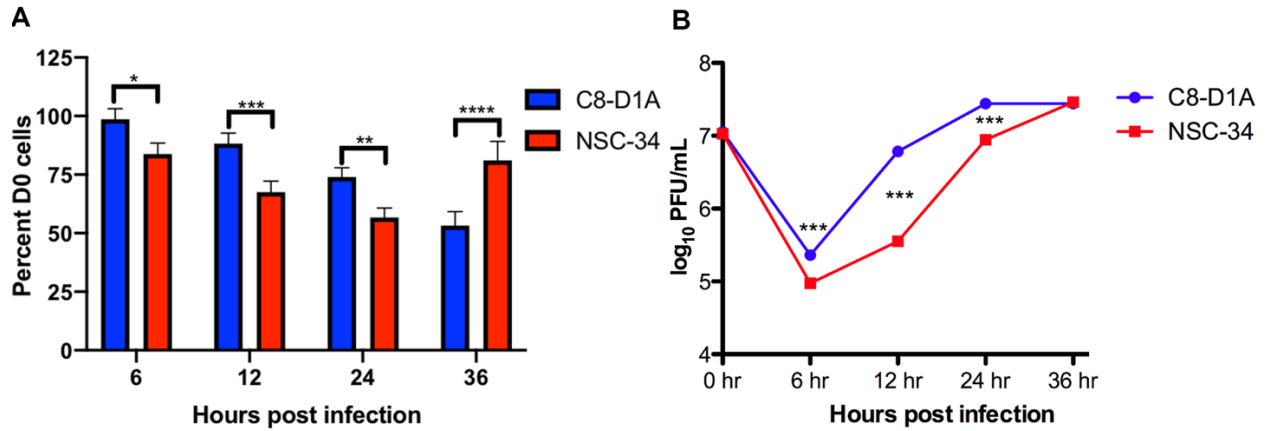


Figure 3.1 Cell Viability and Infectious Virus Produced after CHIKV WT Infection of Astrocytes and Neurons. (A) Cell viability was measured by trypan blue exclusion after infection of C8-D1A and NSC-34 cells with CHIKV 181/25 (WT) at an MOI of 5. (B) Supernatants of C8-D1A cells and NSC-34 cells infected with WT were serially diluted and plated on Vero cells and plaque formation assessed. The data represent the mean \pm SD from three independent experiments. * $P < 0.05$, ** $P < 0.01$, *** $P < 0.001$, **** $P < 0.0001$ (C8-D1A WT vs NSC-34 WT).

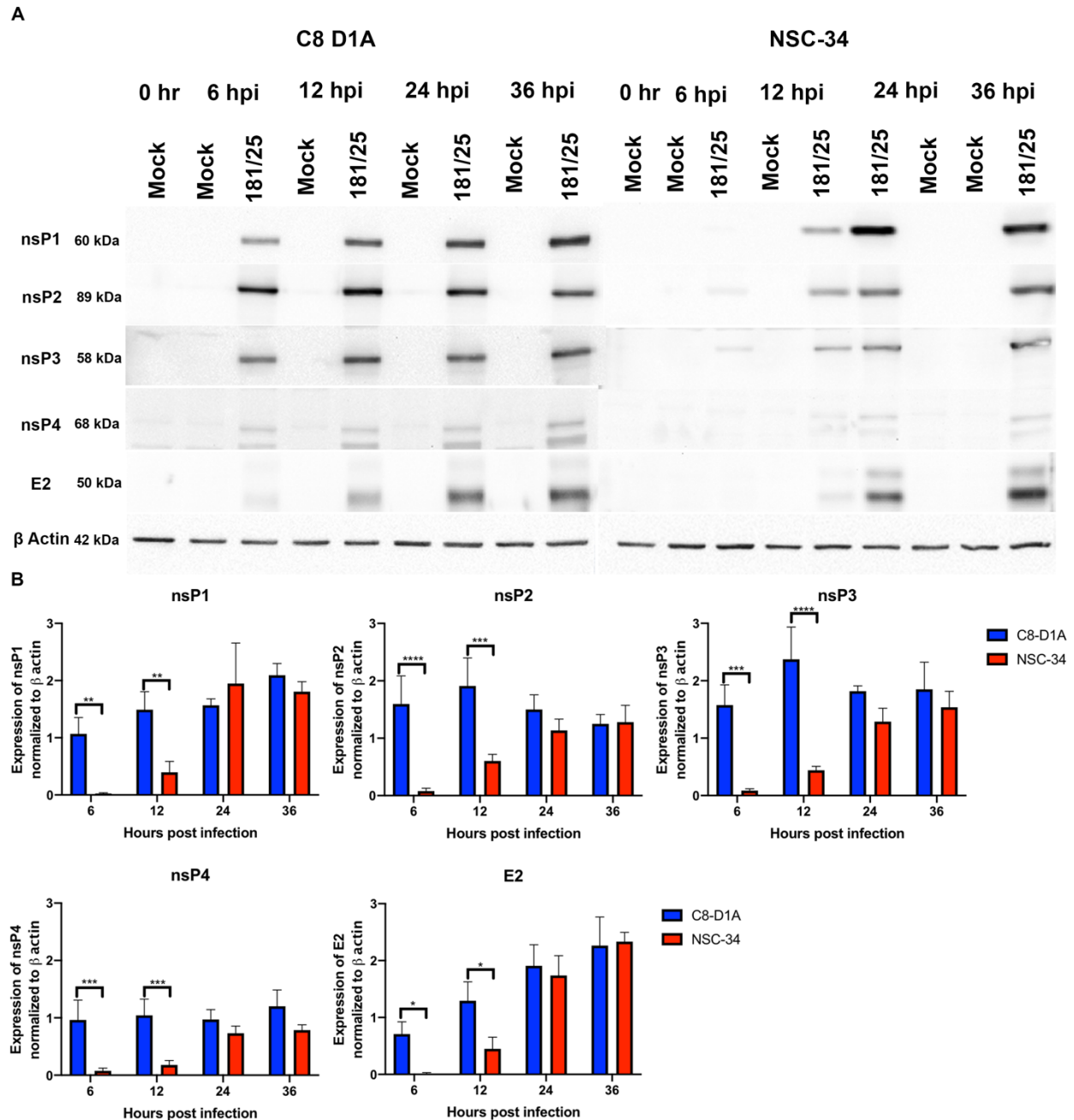


Figure 3.2 Synthesis of CHIKV Proteins by Infected Astrocytes and Neurons. Lysates from C8-D1A and NSC-34 cells infected with CHIKV 181/25 (WT) at an MOI of 5 were immunoblotted with antibodies to nsP1, nsP2, nsP3 nonstructural proteins, E2 structural protein, and β -actin. (A) A representative image from three independent experiments. (B) Quantification by densitometry of viral protein normalized to actin from three independent experiments. Data illustrate the mean \pm SD. * $P < 0.05$, ** $P < 0.01$, *** $P < 0.001$, **** $P < 0.0001$ (C8-D1A WT vs NSC-34 WT).

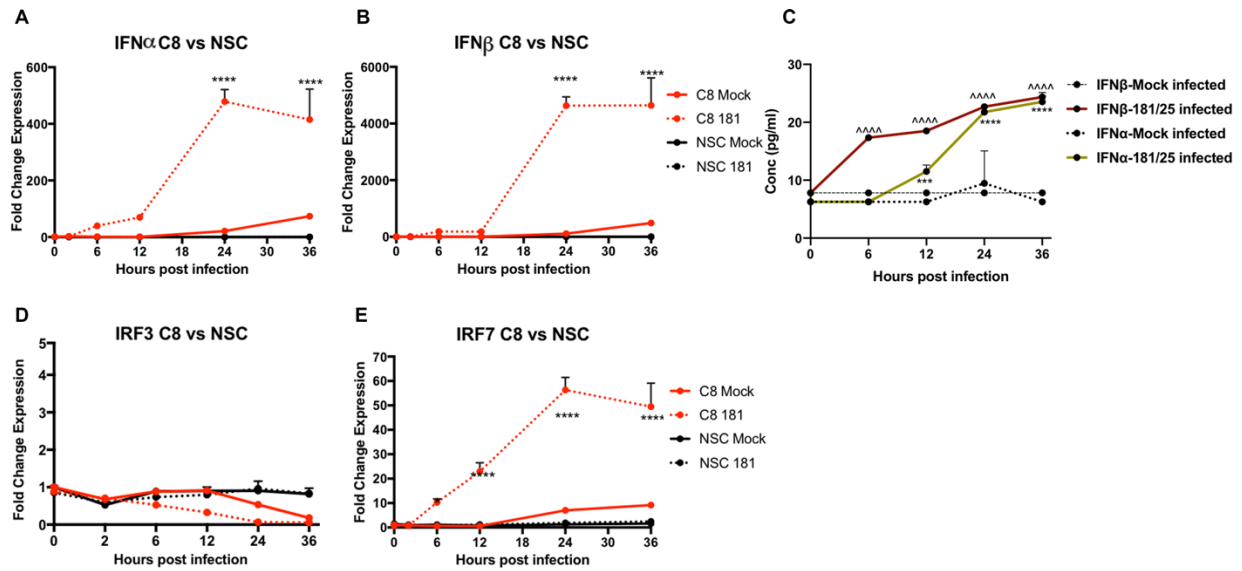


Figure 3.3 Type I IFN response by CHIKV-infected Astrocytes and Neurons. NSC 34 and C8-D1A cells were either mock-infected or infected with CHIKV 181/25 and RNA was isolated, and cDNA synthesized. Real-time PCR was performed for *Ifna* (A), *Ifnb* (B), *Irf3* (D), and *Irf7* (E) to determine changes in gene expression. C_t value for each transcript was normalized to *Gapdh*. Fold change in expression was calculated relative to 0-hour mock-infected samples. Data represent the average \pm SD. **** $P < 0.0001$ (C8-D1A WT vs NSC-34 WT). (C) Supernatants of C8-D1A cells infected with CHIKV 181/25 (WT) were collected and type I IFN level was measured by ELISA. Data represent the average \pm SD. *** $P < 0.001$, **** $P < 0.0001$ (IFN α ; C8-D1A Mock-infected vs. C8-D1A WT); **** $P < 0.0001$ (IFN β ; C8-D1A Mock-infected vs. C8-D1A WT).

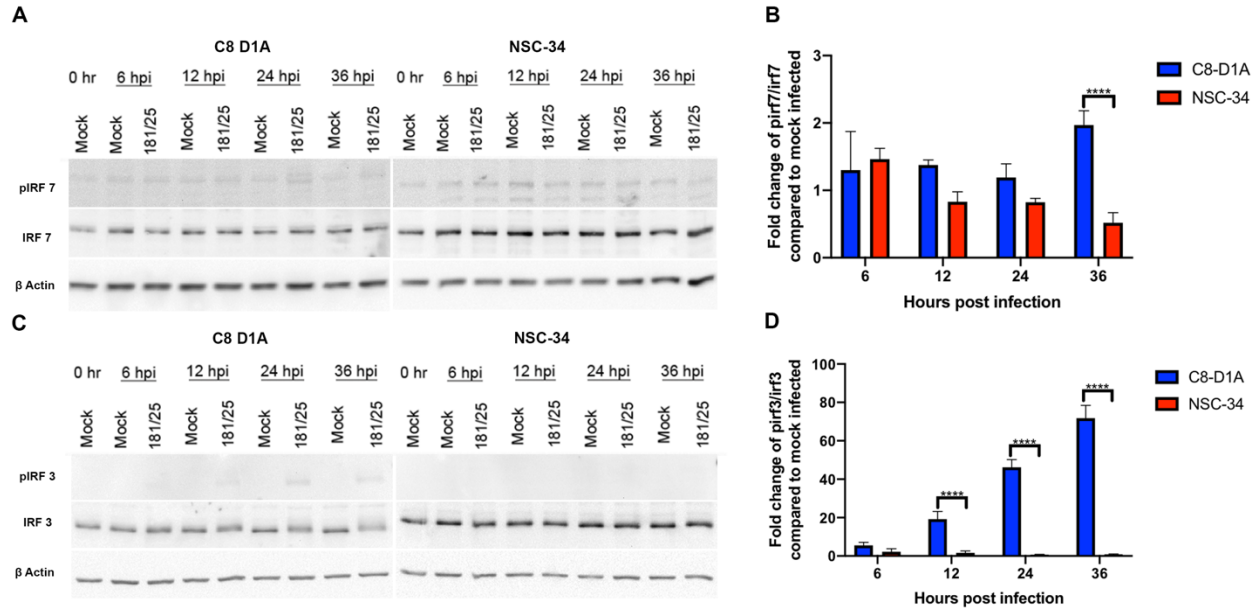


Figure 3.4 Phosphorylation of IRF3 and IRF7 in Astrocytes and Neurons After CHIKV Infection. Lysates from C8-D1A cells and NSC-34 cells infected with CHIKV 181/25 (WT) at an MOI of 5 were immunoblotted for phospho IRF3, IRF3, phospho IRF7, IRF7, and β actin. (A) A representative image from three independent experiments for IRF7 protein expression. (B) The ratio of phosphoIRF7 to total IRF7 was quantified by densitometry and normalized to β actin. (C) A representative image from three independent experiments for IRF3 protein expression. (D) The ratio of phospho IRF3 to total IRF3 was quantified by densitometry and normalized to β actin. **** $P < 0.0001$ (C8-D1A WT vs NSC-34 WT).

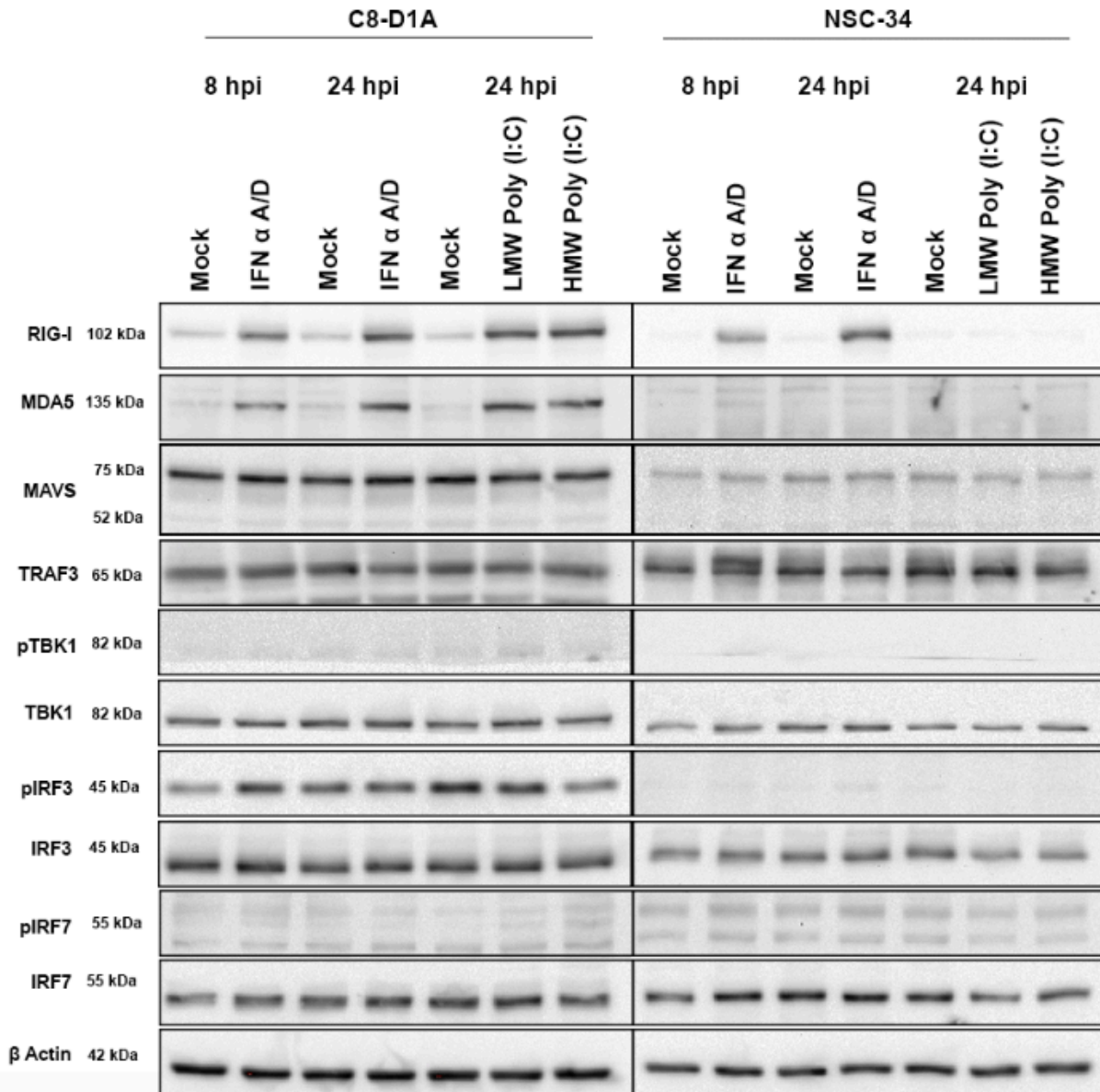


Figure 3.5 RLR Pathway activation by IFN or Poly (I:C) Treatment of Neurons and Astrocytes To activate antiviral PRRs related to Type I IFN, C8-D1A and NSC34 cells were treated with 2 μ l of universal type I IFN (100U/ml) or 10 μ l of LMW and HMW poly (I:C) (1 μ g/ml) in DMEM containing 1% FBS. 24 hours after the treatment, lysates were collected and immunoblots were performed to determine RLR pathway receptor and mediator expression.

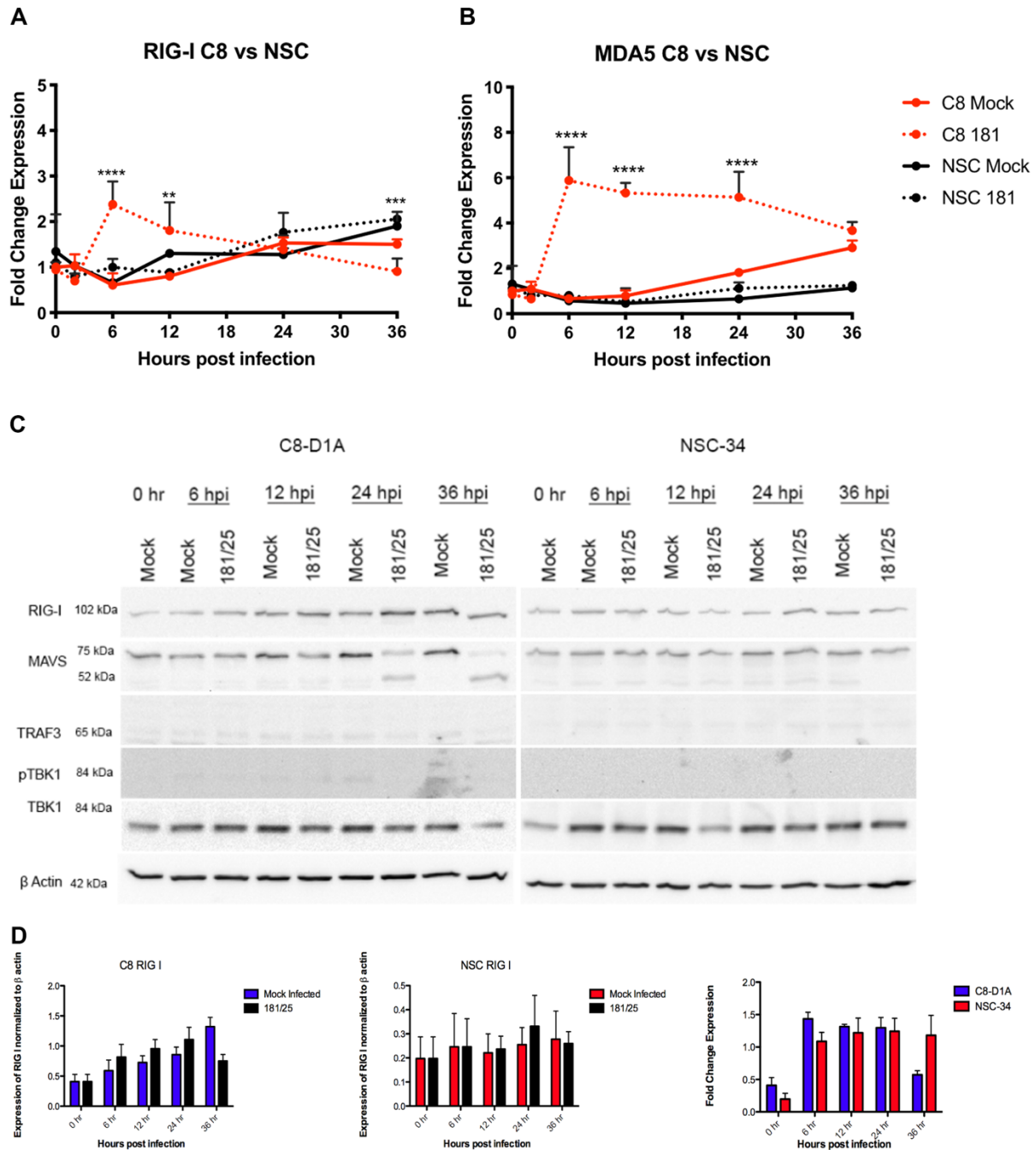


Figure 3.6 RLR Pathway mRNA and Protein in CHIKV-Infected Astrocytes and Neurons NSC-34 and C8-D1A cells were either mock-infected or infected with CHIKV 181/25 at MOI 5 and RNA was isolated, and cDNA synthesized. Gene expression for *Rig-i* (A) and *Mda5* (B) was determined by real-time PCR and C_t values normalized to *Gapdh*. Fold change of expression was calculated by comparison to the 0-hour mock-infected samples. Data show the average \pm SD. ** $P < 0.01$, *** $P < 0.001$, **** $P < 0.0001$ (C8-D1A WT vs NSC-34 WT). (C,D) Lysates from C8-D1A cells and NSC-34 cells infected with CHIKV 181/25 (WT) at an MOI of 5 were immunoblotted for RIG-I, MAVS, TRAF3,

phospho TBK1, TBK1, and β actin. (C) A representative image from three independent experiments. (D) Quantification of RIG-I protein level by densitometry and normalized to actin level from three independent experiments. Data demonstrate the mean \pm SD.

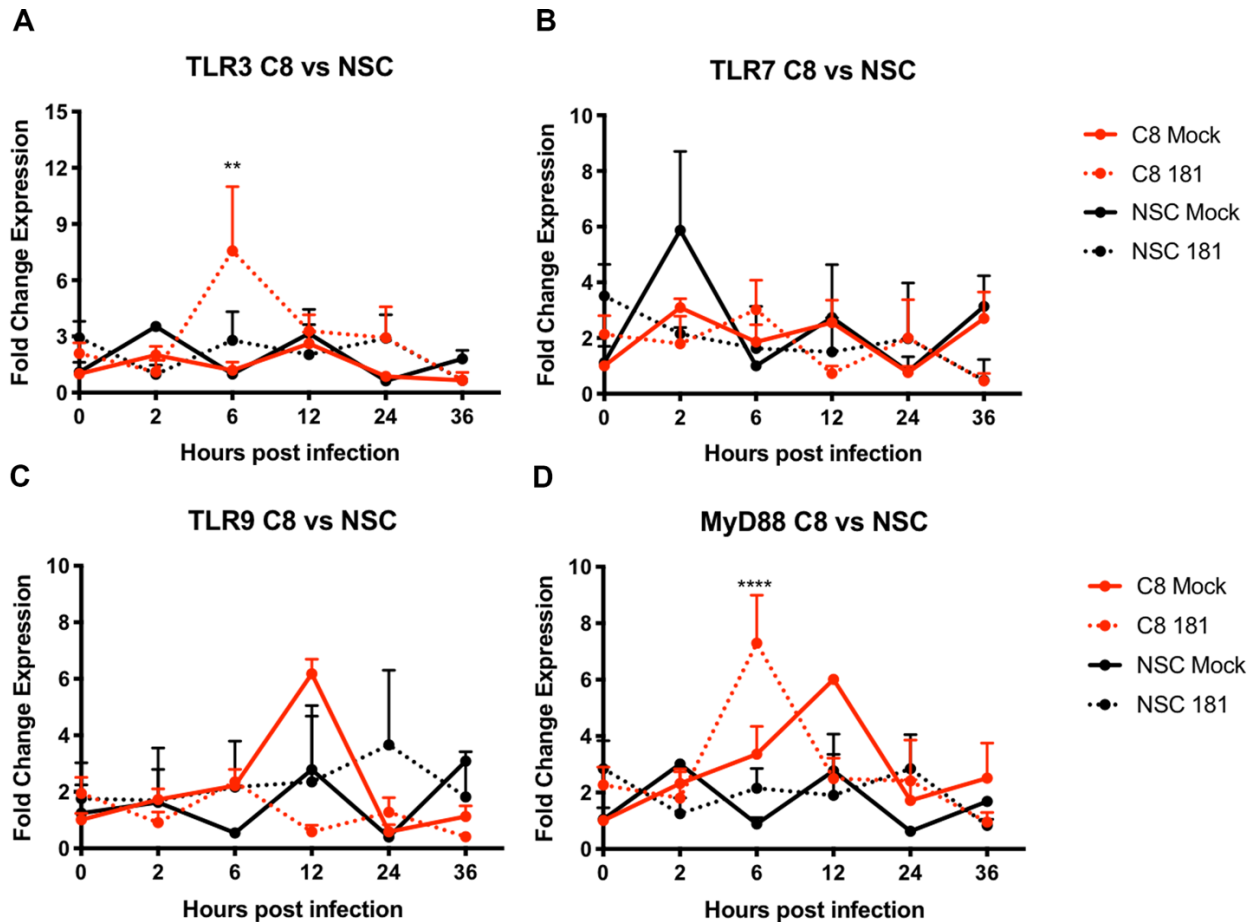


Figure 3.7 Expression of *TLR* mRNAs by CHIKV-Infected Neurons and Astrocytes. NSC-34 and C8-D1A cells were either mock-infected or infected with CHIKV 181/25 at an MOI of 5 and RNA was isolated, and cDNA synthesized. Gene expression for *Tlr3* (A), *Tlr7* (B), *Tlr9* (C), and *Myd88* (D) was determined by real-time PCR and C_t values normalized to *Gapdh*. Fold change in expression was calculated by comparison to the 0-hour mock-infected samples. Data show the average \pm SD. ** $P < 0.01$, **** $P < 0.0001$ (C8-D1A WT vs NSC-34 WT).

3.4 Discussion

Innate immunity is the first line of defense against viral infections. The main roles for innate immunity are identification and restriction of virus replication and activation of the adaptive immune system (47). Early detection of virus is fundamental for activation of anti-viral gene and proteins. TLRs, RLRs, and NLRs are the main PRRs for detection of viral genomes within cells. While the NLR cascade produces inflammatory cytokines like IL1 β , TLR and RLR pathways activate IRF3 and IRF7 to upregulate IFN α and IFN β (50). These type I IFNs bind to receptors to activate its own cells and nearby cells through the Jak/Stat pathway to induce transcription of more antiviral ISGs (54).

In mice model CHIKV antigens are found in both neurons and astrocytes (26, 27). In this study we show that astrocytes produce 3-100 times more infectious virus than neurons (Fig. 3.1 and Fig. 2.1). This correlates with earlier and greater translation of viral nonstructural and structural proteins by astrocytes (Fig. 3.2).

Alphavirus infection increases expression of interferon stimulated PARPs in CNS tissues of mice and in astrocytes, whereas in neuronal cells PARPs are activated for ADP ribosylation of proteins without increased mRNA expression. Upon infection, astrocytes produce type I IFN (Fig. 2.8 and Fig. 3.3A) while neuronal cells do not (70). Animal studies of other neurotrophic viruses have also shown that infected astrocytes rapidly produce type I interferon to restrict virus replication and cytolysis (92). IFN receptor signaling stimulates production of ISGs to restrict and regulate viral blood brain barrier entry (93).

While the TLR pathway leads to the phosphorylation of IRF7, the RLR pathway stimulates phosphorylation of both IRF3 and IRF7. In the current study we demonstrated that neurons could activate only IRF7, whereas astrocytes activated both IRF3 and IRF7

(Fig. 3.4). Transcript levels of *Rig-I* and *Mda5* in astrocytes increase after infection, while in neurons only *Rig-I* increases at later time points. To mimic the dsRNA intermediate formed during infection, astrocytes and neurons were treated with synthetic dsRNA (Fig. 3.5). While astrocytes made RIG-I and MDA5 proteins, neurons did not (Fig. 3.6). Therefore, RLRs are the main signaling pathway leading to type I IFN production by astrocytes and are deficient in neurons.

In summary, MDA-5 and RIG-I detected the dsRNA of CHIKV in astrocytes, but not in neurons. These RLRs activated IRF3 and induced IFN β early after infection in astrocytes. IFN β then induced production of more IRF7 and other ISGs. Although RLR activation lead to restriction of virus replication, unexpectedly, more viral proteins and infectious virus were produced by astrocytes than neurons. More experiments will be required to determine why virus replication is facilitated rather than restricted in astrocytes compared to neurons.

Appendix A: References

1. Jose, J., Snyder, J. E., & Kuhn, R. J. (2009). A structural and functional perspective of alphavirus replication and assembly. *Future microbiology*, 4(7), 837–856. <https://doi.org/10.2217/fmb.09.59>
2. Baxter, V. K., & Heise, M. T. (2018). Genetic control of alphavirus pathogenesis. *Mammalian genome: official journal of the International Mammalian Genome Society*, 29(7-8), 408–424. <https://doi.org/10.1007/s00335-018-9776-1>
3. Tomar, S., Mudgal, R., & Pareek, A. (2018, November 2). RNA-Dependent RNA Polymerase of Alphaviruses: A Potential Target for the Design of Drugs Against Alphaviruses. Retrieved March 10, 2020, from <https://www.sciencedirect.com/science/article/pii/B9780128154229000036>
4. Lwande, O. W., Obanda, V., Bucht, G., Mosomtai, G., Otieno, V., Ahlm, C., & Evander, M. (2015). Global emergence of Alphaviruses that cause arthritis in humans. *Infection ecology & epidemiology*, 5, 29853. <https://doi.org/10.3402/iee.v5.29853>
5. Kraemer, M. U., Sinka, M. E., Duda, K. A., Mylne, A. Q., Shearer, F. M., Barker, C. M., Moore, C. G., Carvalho, R. G., Coelho, G. E., Van Bortel, W., Hendrickx, G., Schaffner, F., Elyazar, I. R., Teng, H. J., Brady, O. J., Messina, J. P., Pigott, D. M., Scott, T. W., Smith, D. L., Wint, G. R., ... Hay, S. I. (2015). The global distribution of the arbovirus vectors *Aedes aegypti* and *Ae. albopictus*. *eLife*, 4, e08347. <https://doi.org/10.7554/eLife.08347>
6. Geographic Distribution. (2019, September 19). Retrieved March 11, 2020, from <https://www.cdc.gov/chikungunya/geo/index.html>
7. Powers A. M. (2017). Vaccine and Therapeutic Options To Control Chikungunya Virus. *Clinical microbiology reviews*, 31(1), e00104-16. <https://doi.org/10.1128/CMR.00104-16>
8. Bleijs, D. A. (2018, May). Chikungunya Epidemiology. Retrieved March 2020, from <http://www.chikungunyavirusnet.com/epidemiology/28-chikungunya-epidemiology.html>
9. Josseran, L., Paquet, C., Zehgnoun, A., Caillere, N., Le Tertre, A., Solet, J. L., & Ledrans, M. (2006). Chikungunya disease outbreak, Reunion Island. *Emerging infectious diseases*, 12(12), 1994–1995. <https://doi.org/10.3201/eid1212.060710>
10. Bessaud, M., Peyrefitte, C. N., Pastorino, B. A., Tock, F., Merle, O., Colpart, J. J., Dehecq, J. S., Girod, R., Jaffar-Bandjee, M. C., Glass, P. J., Parker, M., Tolou, H. J., & Grandadam, M. (2006). Chikungunya virus strains, Reunion Island outbreak. *Emerging infectious diseases*, 12(10), 1604–1606. <https://doi.org/10.3201/eid1210.060596>
11. Kraemer, M., Reiner, R. C., Jr, Brady, O. J., Messina, J. P., Gilbert, M., Pigott, D. M., Yi, D., Johnson, K., Earl, L., Marczak, L. B., Shirude, S., Davis Weaver, N., Bisanzio, D., Perkins, T. A., Lai, S., Lu, X., Jones, P., Coelho, G. E., Carvalho, R. G., Van Bortel, W., ... Golding, N. (2019). Past and future spread of the arbovirus vectors *Aedes aegypti* and *Aedes albopictus*. *Nature microbiology*, 4(5), 854–863. <https://doi.org/10.1038/s41564-019-0376-y>

12. Reinhold, J. M., Lazzari, C. R., & Lahondère, C. (2018). Effects of the Environmental Temperature on *Aedes aegypti* and *Aedes albopictus* Mosquitoes: A Review. *Insects*, 9(4), 158. <https://doi.org/10.3390/insects9040158>
13. Silva, L. A., & Dermody, T. S. (2017). Chikungunya virus: epidemiology, replication, disease mechanisms, and prospective intervention strategies. *The Journal of clinical investigation*, 127(3), 737–749. <https://doi.org/10.1172/JCI84417>
14. Trotochaud, M. (2019, August 22). Chikungunya Around the World. Retrieved March 2020, from <https://www.outbreakobservatory.org/outbreakthursday-1/8/22/2019/chikungunya-around-the-world>
15. Thiberville, S.-D., Moyen, N., Dupuis-Maguiraga, L., Nougairede, A., Gould, E. A., Roques, P., & Lamballerie, X. D. (2013). Chikungunya fever: Epidemiology, clinical syndrome, pathogenesis, and therapy. *Antiviral Research*, 99(3), 345–370. doi: 10.1016/j.antiviral.2013.06.009
16. Rudolph, K. E., Lessler, J., Moloney, R. M., Kmush, B., & Cummings, D. A. (2014). Incubation periods of mosquito-borne viral infections: a systematic review. *The American journal of tropical medicine and hygiene*, 90(5), 882–891. <https://doi.org/10.4269/ajtmh.13-0403>
17. Galán-Huerta, K., Rivas-Estilla, A., Fernández-Salas, I., Farfan-Ale, J., & Ramos-Jiménez, J. (2015). Chikungunya virus: A general overview. *Medicina Universitaria*, 17(68), 175–183. doi: 10.1016/j.rmu.2015.06.001
18. Nkoghe, D., Kassa, R. F., Caron, M., Grard, G., Mombo, I., Bikié, B., Paupy, C., Becquart, P., Bisvigou, U., & Leroy, E. M. (2012). Clinical forms of chikungunya in Gabon, 2010. *PLoS neglected tropical diseases*, 6(2), e1517. <https://doi.org/10.1371/journal.pntd.0001517>
19. Staikowsky, F., Talarmin, F., Grivard, P., Souab, A., Schuffenecker, I., Le Roux, K., Lecuit, M., & Michault, A. (2009). Prospective study of Chikungunya virus acute infection in the Island of La Réunion during the 2005-2006 outbreak. *PloS one*, 4(10), e7603. <https://doi.org/10.1371/journal.pone.0007603>
20. Staikowsky, F., Le Roux, K., Schuffenecker, I., Laurent, P., Grivard, P., Develay, A., & Michault, A. (2008). Retrospective survey of Chikungunya disease in Réunion Island hospital staff. *Epidemiology and infection*, 136(2), 196–206. <https://doi.org/10.1017/S0950268807008424>
21. Thiberville, S. D., Boisson, V., Gaudart, J., Simon, F., Flahault, A., & de Lamballerie, X. (2013). Chikungunya fever: a clinical and virological investigation of outpatients on Reunion Island, South-West Indian Ocean. *PLoS neglected tropical diseases*, 7(1), e2004. <https://doi.org/10.1371/journal.pntd.0002004>
22. Morrison, C. R., Plante, K. S., & Heise, M. T. (2016). Chikungunya Virus: Current Perspectives on a Reemerging Virus. *Microbiology spectrum*, 4(3), 10.1128/microbiolspec.EI10-0017-2016.
23. Mehta, R., Gerardin, P., de Brito, C., Soares, C. N., Ferreira, M., & Solomon, T. (2018). The neurological complications of chikungunya virus: A systematic review. *Reviews in medical virology*, 28(3), e1978. <https://doi.org/10.1002/rmv.1978>
24. Singh, S. S., Manimunda, S. P., Sugunan, A. P., Sahina, & Vijayachari, P. (2008). Four cases of acute flaccid paralysis associated with chikungunya virus

- infection. *Epidemiology and infection*, 136(9), 1277–1280.
<https://doi.org/10.1017/S0950268807009739>
25. Griffin D. E. (2011). Viral encephalomyelitis. *PLoS pathogens*, 7(3), e1002004.
<https://doi.org/10.1371/journal.ppat.1002004>
 26. Matusali, G., Colavita, F., Bordi, L., Lalle, E., Ippolito, G., Capobianchi, M. R., & Castilletti, C. (2019). Tropism of the Chikungunya Virus. *Viruses*, 11(2), 175.
<https://doi.org/10.3390/v11020175>
 27. Chiam, C. W., Chan, Y. F., Ong, K. C., Wong, K. T., & Sam, I. (2015). Neurovirulence comparison of Chikungunya virus isolates of the Asian and East/Central/South african Genotypes from Malaysia. *Journal of General Virology*, 96(11), 3243-3254. doi:10.1099/jgv.0.000263
 28. Das, T., Hoarau, J. J., Bandjee, M. C., Maquart, M., & Gasque, P. (2015). Multifaceted innate immune responses engaged by astrocytes, microglia and resident dendritic cells against chikungunya neuroinfection. *Journal of General Virology*, 96(2), 294-310. doi:10.1099/vir.0.071175-0
 29. Potokar, M., Jorgačevski, J., & Zorec, R. (2019). Astrocytes in Flavivirus Infections. *International journal of molecular sciences*, 20(3), 691.
<https://doi.org/10.3390/ijms20030691>
 30. Levine, B., Hardwick, J. M., & Griffin, D. E. (1994). Persistence of alphaviruses in vertebrate hosts. *Trends in Microbiology*, 2(1), 25-28. doi:10.1016/0966-842x(94)90341-7
 31. Brown, R. S., Wan, J. J., & Kielian, M. (2018). The Alphavirus Exit Pathway: What We Know and What We Wish We Knew. *Viruses*, 10(2), 89.
<https://doi.org/10.3390/v10020089>
 32. Singh, S. K., & Unni, S. K. (2011, March). Chikungunya virus: host pathogen interaction. Retrieved March 2020, from
<https://www.ncbi.nlm.nih.gov/pubmed/21412934>
 33. Das, P. K., Puusepp, L., Varghese, F. S., Utt, A., Ahola, T., Kananovich, D. G., Lopp, M., Merits, A., & Karelson, M. (2016). Design and Validation of Novel Chikungunya Virus Protease Inhibitors. *Antimicrobial agents and chemotherapy*, 60(12), 7382–7395. <https://doi.org/10.1128/AAC.01421-16>
 34. Chevillon, C., Briant, L., Renaud, F., & Devaux, C. (2008). The Chikungunya threat: an ecological and evolutionary perspective. *Trends in Microbiology*, 16(2), 80–88. doi: 10.1016/j.tim.2007.12.003
 35. Hyde, J. L., Chen, R., Trobaugh, D. W., Diamond, M. S., Weaver, S. C., Klimstra, W. B., & Wilusz, J. (2015). The 5' and 3' ends of alphavirus RNAs--Non-coding is not non-functional. *Virus research*, 206, 99–107.
<https://doi.org/10.1016/j.virusres.2015.01.016>
 36. Hardy, R. W., & Rice, C. M. (2005). Requirements at the 3' end of the sindbis virus genome for efficient synthesis of minus-strand RNA. *Journal of virology*, 79(8), 4630–4639. <https://doi.org/10.1128/JVI.79.8.4630-4639.2005>
 37. Trobaugh, D. W., Gardner, C. L., Sun, C., Haddow, A. D., Wang, E., Chapnik, E., Mildner, A., Weaver, S. C., Ryman, K. D., & Klimstra, W. B. (2014). RNA viruses can hijack vertebrate microRNAs to suppress innate immunity. *Nature*, 506(7487), 245–248. <https://doi.org/10.1038/nature12869>

38. Strauss, J. H., & Strauss, E. G. (1994). The alphaviruses: gene expression, replication, and evolution. *Microbiological reviews*, 58(3), 491–562.
39. Nieva, J., & Carrasco, L. (2015). Viroporins: Structures and functions beyond cell membrane permeabilization. *Viruses*, 7(10), 5169–5171. doi: 10.3390/v7102866
40. Sanz, M. A., Rejas, M. T., & Carrasco, L. (2003). Individual Expression of Sindbis Virus Glycoproteins. E1 Alone Promotes Cell Fusion. *Virology*, 305(2), 463–472. doi: 10.1006/viro.2002.1771
41. Bernard, E., Solignat, M., Gay, B., Chazal, N., Higgs, S., Devaux, C., & Briant, L. (2010). Endocytosis of chikungunya virus into mammalian cells: role of clathrin and early endosomal compartments. *PloS one*, 5(7), e11479. <https://doi.org/10.1371/journal.pone.0011479>
42. Ooi, Y. S., Stiles, K. M., Liu, C. Y., Taylor, G. M., & Kielian, M. (2013). Genome-wide RNAi screen identifies novel host proteins required for alphavirus entry. *PLoS pathogens*, 9(12), e1003835. <https://doi.org/10.1371/journal.ppat.1003835>
43. Lee, R. C., Hapuarachchi, H. C., Chen, K. C., Hussain, K. M., Chen, H., Low, S. L., Ng, L. C., Lin, R., Ng, M. M., & Chu, J. J. (2013). Mosquito cellular factors and functions in mediating the infectious entry of chikungunya virus. *PLoS neglected tropical diseases*, 7(2), e2050. <https://doi.org/10.1371/journal.pntd.0002050>
44. Hoornweg, T. E., Duijl-Richter, M. K. S. V., Nuñez, N. V. A., Albuлесcu, I. C., Hemert, M. J. V., & Smit, J. M. (2016). Dynamics of Chikungunya Virus Cell Entry Unraveled by Single-Virus Tracking in Living Cells. *Journal of Virology*, 90(9), 4745–4756. doi: 10.1128/jvi.03184-15
45. Spuul, P., Balistreri, G., Hellström, K., Golubtsov, A. V., Jokitalo, E., & Ahola, T. (2011). Assembly of alphavirus replication complexes from RNA and protein components in a novel trans-replication system in mammalian cells. *Journal of virology*, 85(10), 4739–4751. <https://doi.org/10.1128/JVI.00085-11>
46. Zhang, Y., Corver, J., Chipman, P. R., Zhang, W., Pletnev, S. V., Sedlak, D., Baker, T. S., Strauss, J. H., Kuhn, R. J., & Rossmann, M. G. (2003). Structures of immature flavivirus particles. *The EMBO journal*, 22(11), 2604–2613. <https://doi.org/10.1093/emboj/cdq270>
47. Long, K. M., & Heise, M. T. (2015). Protective and Pathogenic Responses to Chikungunya Virus Infection. *Current tropical medicine reports*, 2(1), 13–21. <https://doi.org/10.1007/s40475-015-0037-z>
48. Libbey, J. E., & Fujinami, R. S. (2014). Adaptive immune response to viral infections in the central nervous system. *Handbook of clinical neurology*, 123, 225–247. <https://doi.org/10.1016/B978-0-444-53488-0.00010-9>
49. Flint, S. J., Enquist, L. W., Racaniello, V. R., Rall, G. F., & Skalka, A. M. (2015). Chapter 3. In *Principles of virology*. Washington, D.C.: ASM Press.
50. Heaton, S. M., Borg, N. A., & Dixit, V. M. (2016). Ubiquitin in the activation and attenuation of innate antiviral immunity. *The Journal of experimental medicine*, 213(1), 1–13. <https://doi.org/10.1084/jem.20151531>
51. Ertl, H. C. (2013). Immunity to Viruses. In *Fundamental Immunology* (pp. 937-972). Philadelphia, PA: Lippincott, Williams & Wilkins.
52. Fox, J. M., & Diamond, M. S. (2016). Immune-Mediated Protection and Pathogenesis of Chikungunya Virus. *Journal of immunology (Baltimore, Md. : 1950)*, 197(11), 4210–4218. <https://doi.org/10.4049/jimmunol.1601426>

53. Rudd, P. A., Wilson, J., Gardner, J., Larcher, T., Babarit, C., Le, T. T., Anraku, I., Kumagai, Y., Loo, Y. M., Gale, M., Jr, Akira, S., Khromykh, A. A., & Suhrbier, A. (2012). Interferon response factors 3 and 7 protect against Chikungunya virus hemorrhagic fever and shock. *Journal of virology*, 86(18), 9888–9898. <https://doi.org/10.1128/JVI.00956-12>
54. Nan, Y., Wu, C., & Zhang, Y. J. (2017). Interplay between Janus Kinase/Signal Transducer and Activator of Transcription Signaling Activated by Type I Interferons and Viral Antagonism. *Frontiers in immunology*, 8, 1758. <https://doi.org/10.3389/fimmu.2017.01758>
55. Morales, D. J., & Lenschow, D. J. (2013). The antiviral activities of ISG15. *Journal of molecular biology*, 425(24), 4995–5008. <https://doi.org/10.1016/j.jmb.2013.09.041>
56. Werneke, S. W., Schilte, C., Rohatgi, A., Monte, K. J., Michault, A., Arenzana-Seisdedos, F., Vanlandingham, D. L., Higgs, S., Fontanet, A., Albert, M. L., & Lenschow, D. J. (2011). ISG15 is critical in the control of Chikungunya virus infection independent of UbE1L mediated conjugation. *PLoS pathogens*, 7(10), e1002322. <https://doi.org/10.1371/journal.ppat.1002322>
57. Thompson, W. L., & Van Eldik, L. J. (2009). Inflammatory cytokines stimulate the chemokines CCL2/MCP-1 and CCL7/MCP-3 through NFκB and MAPK dependent pathways in rat astrocytes [corrected]. *Brain research*, 1287, 47–57. <https://doi.org/10.1016/j.brainres.2009.06.081>
58. Teo, Lum, F., Claser, C., Lulla, V., Lulla, A., Merits, A., . . . Ng, L. F. (2012). A Pathogenic Role for CD4+ T Cells during Chikungunya Virus Infection in Mice. *The Journal of Immunology*, 190(1), 259-269. doi:10.4049/jimmunol.1202177
59. Feibelman, K. M., Fuller, B. P., Li, L., LaBarbera, D. V., & Geiss, B. J. (2018). Identification of small molecule inhibitors of the Chikungunya virus nsP1 RNA capping enzyme. *Antiviral research*, 154, 124–131. <https://doi.org/10.1016/j.antiviral.2018.03.013>
60. Ahola, T., & Kääriäinen, L. (1995). Reaction in alphavirus mRNA capping: formation of a covalent complex of nonstructural protein nsP1 with 7-methyl-GMP. *Proceedings of the National Academy of Sciences of the United States of America*, 92(2), 507–511. <https://doi.org/10.1073/pnas.92.2.507>
61. Strauss, E. G., Groot, R. J. D., Levinson, R., & Strauss, J. H. (1992). Identification of the active site residues in the nsP2 proteinase of sindbis virus. *Virology*, 191(2), 932–940. doi: 10.1016/0042-6822(92)90268-t
62. Götte, B., Liu, L., & McInerney, G. M. (2018). The Enigmatic Alphavirus Non-Structural Protein 3 (nsP3) Revealing Its Secrets at Last. *Viruses*, 10(3), 105. <https://doi.org/10.3390/v10030105>
63. Fros, J. J., Domeradzka, N. E., Baggen, J., Geertsema, C., Flipse, J., Vlak, J. M., & Pijlman, G. P. (2012). Chikungunya Virus nsP3 Blocks Stress Granule Assembly by Recruitment of G3BP into Cytoplasmic Foci. *Journal of Virology*, 86(19), 10873–10879. doi: 10.1128/jvi.01506-12
64. Gorchakov, R., Garmashova, N., Frolova, E., & Frolov, I. (2008). Different types of nsP3-containing protein complexes in Sindbis virus-infected cells. *Journal of virology*, 82(20), 10088–10101. <https://doi.org/10.1128/JVI.01011-08>

65. Cristea, I. M., Carroll, J.-W. N., Rout, M. P., Rice, C. M., Chait, B. T., & Macdonald, M. R. (2006). Tracking and Elucidating Alphavirus -Host Protein Interactions. *Journal of Biological Chemistry*, 281(40), 30269–30278. doi: 10.1074/jbc.m603980200
66. Buchan, J. R., & Parker, R. (2009). Eukaryotic stress granules: the ins and outs of translation. *Molecular cell*, 36(6), 932–941. <https://doi.org/10.1016/j.molcel.2009.11.020>
67. White, J. P., & Lloyd, R. E. (2012). Regulation of stress granules in virus systems. *Trends in microbiology*, 20(4), 175–183. <https://doi.org/10.1016/j.tim.2012.02.001>
68. Leung, A., McPherson, R. L., & Griffin, D. E. (2018). Macrodomein ADP-ribosylhydrolase and the pathogenesis of infectious diseases. *PLoS pathogens*, 14(3), e1006864. <https://doi.org/10.1371/journal.ppat.1006864>
69. Rack G., Perina, D., & Ahel, I. (2016). Macrodomeins: Structure, function, evolution, and catalytic activities. *Annual Review of Biochemistry*, 85(1), 431-454. doi:10.1146/annurev-biochem-060815-014935
70. Mclennan G. (2005). The Nudix hydrolase superfamily. *Cellular and Molecular Life Sciences*, 63(2), 123-143. doi:10.1007/s00018-005-5386-7
71. Chen, D., Vollmar, M., Rossi, M. N., Phillips, C., Kraehenbuehl, R., Slade, D., Mehrotra, P. V., von Delft, F., Crosthwaite, S. K., Gileadi, O., Denu, J. M., & Ahel, I. (2011). Identification of macrodomein proteins as novel O-acetyl-ADP-ribose deacetylases. *The Journal of biological chemistry*, 286(15), 13261–13271. <https://doi.org/10.1074/jbc.M110.206771>
72. McPherson, R. L., Abraham, R., Sreekumar, E., Ong, S. E., Cheng, S. J., Baxter, V. K., Kistemaker, H. A., Filippov, D. V., Griffin, D. E., & Leung, A. K. (2017). ADP-ribosylhydrolase activity of Chikungunya virus macrodomein is critical for virus replication and virulence. *Proceedings of the National Academy of Sciences of the United States of America*, 114(7), 1666–1671. <https://doi.org/10.1073/pnas.1621485114>
73. Abraham, R., Hauer, D., McPherson, R. L., Utt, A., Kirby, I. T., Cohen, M. S., Merits, A., Leung, A., & Griffin, D. E. (2018). ADP-ribosyl-binding and hydrolase activities of the alphavirus nsP3 macrodomein are critical for initiation of virus replication. *Proceedings of the National Academy of Sciences of the United States of America*, 115(44), E10457–E10466. <https://doi.org/10.1073/pnas.1812130115>
74. Abraham, R., McPherson, R. L., Dasovich, M., Badiee, M., Leung, A., & Griffin, D. E. (2020). Both ADP-Ribosyl-Binding and Hydrolase Activities of the Alphavirus nsP3 Macrodomein Affect Neurovirulence in Mice. *mBio*, 11(1), e03253-19. <https://doi.org/10.1128/mBio.03253-19>
75. Park, E., & Griffin, D. E. (2009). The nsP3 macro domein is important for Sindbis virus replication in neurons and neurovirulence in mice. *Virology*, 388(2), 305–314. <https://doi.org/10.1016/j.virol.2009.03.031>
76. Liu, C., & Yu, X. (2015). ADP-ribosyltransferases and poly ADP-ribosylation. *Current protein & peptide science*, 16(6), 491–501. <https://doi.org/10.2174/1389203716666150504122435>

77. Daniels, C. M., Ong, S. E., & Leung, A. K. (2014). Phosphoproteomic approach to characterize protein mono- and poly(ADP-ribosyl)ation sites from cells. *Journal of proteome research*, 13(8), 3510–3522. <https://doi.org/10.1021/pr401032q>
78. Gupte, Liu, Z., & Kraus, W. L. (2017). PARPs and ADP-RIBOSYLATION: Recent ADVANCES linking molecular functions to biological outcomes. *Genes & Development*, 31(2), 101-126. doi:10.1101/gad.291518.116
79. O'Sullivan, J., Tedim Ferreira, M., Gagné, J. P., Sharma, A. K., Hendzel, M. J., Masson, J. Y., & Poirier, G. G. (2019). Emerging roles of eraser enzymes in the dynamic control of protein ADP-ribosylation. *Nature communications*, 10(1), 1182. <https://doi.org/10.1038/s41467-019-08859-x>
80. Luo, X., & Kraus, W. L. (2012). On par WITH Parp: Cellular stress signaling through poly(ADP-ribose) AND PARP-1. *Genes & Development*, 26(5), 417-432. doi:10.1101/gad.183509.111
81. Devalaraja-Narashimha, & Padanilam, B. J. (2010). PARP1 deficiency exacerbates diet-induced obesity in mice. *Journal of Endocrinology*, 205(3), 243-252. doi:10.1677/joe-09-0402
82. Leung, Vyas, S., Rood, J., Bhutkar, A., Sharp, P., & Chang, P. (2011). Poly(adp-ribose) regulates stress responses and microrna activity in the cytoplasm. *Molecular Cell*, 42(4), 489-499. doi:10.1016/j.molcel.2011.04.015
83. Huang, J. Y., Wang, K., Vermehren-Schmaedick, A., Adelman, J. P., & Cohen, M. S. (2016). PARP6 is a Regulator of Hippocampal Dendritic Morphogenesis. *Scientific reports*, 6, 18512. <https://doi.org/10.1038/srep18512>
84. Kuny, C. V., & Sullivan, C. S. (2016). Virus-Host Interactions and the ARTD/PARP Family of Enzymes. *PLoS pathogens*, 12(3), e1005453. <https://doi.org/10.1371/journal.ppat.1005453>
85. Gao, G. (2002). Inhibition of Retroviral RNA Production by ZAP, a CCCH-Type Zinc Finger Protein. *Science*, 297(5587), 1703–1706. doi: 10.1126/science.1074276
86. Cummins, N., & Badley, A. (2009). The TRAIL to viral pathogenesis: the good, the bad and the ugly. *Current molecular medicine*, 9(4), 495–505. <https://doi.org/10.2174/156652409788167078>
87. Fehr, A. R., Singh, S. A., Kerr, C. M., Mukai, S., Higashi, H., & Aikawa, M. (2020). The impact of PARPs and ADP-ribosylation on inflammation and host–pathogen interactions. *Genes & Development*, 34(5-6), 341–359. doi: 10.1101/gad.334425.119
88. Sofroniew, M. V., & Vinters, H. V. (2010). Astrocytes: biology and pathology. *Acta neuropathologica*, 119(1), 7–35. <https://doi.org/10.1007/s00401-009-0619-8>
89. Gorchakov, R., Wang, E., Leal, G., Forrester, N. L., Plante, K., Rossi, S. L., Partidos, C. D., Adams, A. P., Seymour, R. L., Weger, J., Borland, E. M., Sherman, M. B., Powers, A. M., Osorio, J. E., & Weaver, S. C. (2012). Attenuation of Chikungunya virus vaccine strain 181/clone 25 is determined by two amino acid substitutions in the E2 envelope glycoprotein. *Journal of virology*, 86(11), 6084–6096. <https://doi.org/10.1128/JVI.06449-11>
90. Utt, A., Quirin, T., Saul, S., Hellström, K., Ahola, T., & Merits, A. (2016). Versatile Trans-Replication Systems for Chikungunya Virus Allow Functional Analysis and

Tagging of Every Replicase Protein. *PloS one*, 11(3), e0151616.
<https://doi.org/10.1371/journal.pone.0151616>

91. Cashman, N. R., Durham, H. D., Blusztajn, J. K., Oda, K., Tabira, T., Shaw, I. T., . . . Antel, J. P. (1992). Neuroblastoma × spinal cord (NSC) hybrid cell lines resemble developing motor neurons. *Developmental Dynamics*, 194(3), 209-221. doi:10.1002/aja.1001940306
92. Lindqvist, R., Mundt, F., Gilthorpe, J. D., Wölfel, S., Gekara, N. O., Kröger, A., & Överby, A. K. (2016). Fast type I interferon response protects astrocytes from flavivirus infection and virus-induced cytopathic effects. *Journal of neuroinflammation*, 13(1), 277. <https://doi.org/10.1186/s12974-016-0748-7>
93. Daniels, B. P., Jujjavarapu, H., Durrant, D. M., Williams, J. L., Green, R. R., White, J. P., Lazear, H. M., Gale, M., Jr, Diamond, M. S., & Klein, R. S. (2017). Regional astrocyte IFN signaling restricts pathogenesis during neurotropic viral infection. *The Journal of clinical investigation*, 127(3), 843–856. <https://doi.org/10.1172/JCI88720>
- 94.

Appendix B: Curriculum Vitae

TAEWOO KIM

1101 N. Calvert Street Room 1004, Baltimore, MD, 21202 Email: tkim96@jhmi.edu Phone: (510) 701-9750
Foreign Address: Lotte Castle 2danji 208dong 1704ho, 46 Sinseon-ro, Nam-gu, Ulsan, South Korea, 44763

EDUCATION

University of California, Berkeley

Bachelor of Arts, Molecular and Cell Biology, Immunology Emphasis,

May 2017

Johns Hopkins University, School of Public Health

ScM, Molecular Microbiology, and Immunology,

GPA: 4.0

Estimates on May 2020

RESEARCH EXPERIENCE

Korea University ChanWha Kim LAB

Diabetic team Research Assistant

40 hours/week

Summer 2010, 2011

- Renoprotective effect is induced by PI3K inhibitor on proteinuric renal disease rats
- Techniques: Mouse modeling, ELISA, Western blotting, Immunofluorescence, Renal pathology

Cancer Stem cell team Research Assistant

40 hours/week

Summer 2012, 2013

- Dual blocking of PI3K and mTOR improves chemotherapeutic effects on SW620 Human colorectal cancer stem cells
- Techniques: FACS, RNA isolation, semi-quantitative RT-PCR, Cell viability assay, IF analysis

Optical team Research Assistant

40 hours/week

Summer 2014

- Conditioned medium of human bone marrow stem cells attenuates IL-1 derived inflammation in corneal epithelial cells
- Techniques: Human bone marrow stem cell culture, THP-1 differentiation, FACS, ELISA

UC Berkeley Barcellos' Genetic Epidemiology and Genomics Lab,

Research Volunteer

12 hours/week

Aug 2016 - May 2017

Research Affiliate

20 hours/week

May 2017 – April 2018

- Processing of human biospecimens, including whole blood, buffy coats, serum, plasma, blood clots, saliva, sorted cells, and solid tissues/glands. DNA/RNA extraction, quantitation, and plating. DNA methylation, DNA microarray

JHSPH Diane Griffin's Lab

Master student

Nov 2018- present

- ADP-ribosyl binding and hydrolase activities of the alphavirus nsP3 macrodomain are critical for the initiation of virus replication at astrocytic cells
- Technique: FACS, Plaque assay, Western blot, Plasmid Preparation, CRISPR/Cas 9, Radioactive material labeling, trans-replicase system

TEACHING EXPERIENCE

Teracle Inc.

Lecturer

3 hours/week

March 2016 – August 2016

- Filmed 10 Basic Immunology lectures for high school and college students
- 3D presentation of molecules and samples under the light board

Basic cGMP Workshop led by Korea Government

Teaching Assistant

35 hours/workshop

Summer 2010, 2011, 2014

- Approval Process for Drugs and Biologics
- cGMP Facility Design for Vaccines
- Sterilization Processes and International GMP Inspection

SKILLS AND LANGUAGE

Biology Laboratory Procedures

- Cell culturing, qPCR, RT-PCR, immunofluorescence, PCR, Gel Electrophoresis, DNA Sequencing, basic Bioinformatics (NCBI, OMIM, BLAST, etc.), ANOVA

Language

- Fluent in Korean and English

Microsoft Program

- Advanced statistical modeling using Excel, Prism 7,8

AWARDS/ CERTIFICATES

cGMP Certificate by Korea Government	Summer 2009
General Douglas MacArthur Award	May 2013
Vaccine Science and Policy Certificate	May 2019
Good Clinical Practice: A vaccine trials prospective	May 2019

EXTRACURRICULARS

Korea University Hospital Volunteer

Volunteer on Patient Support Team	65 hours/Summer	Summer 2010, 2011
· Book lending service to patients		
· Support elderly patients for prescription from machines		
· Translator for international patients from Korea		
Volunteer on Pediatric Team	65 hours/Summer	Summer 2012, 2014
· Measured temperature, height, weight, and head size for babies		

Sigma Mu Delta Premedical Fraternity

Fall 2013 - Fall 2015

Academic Vice President	8 hours/week	Spring - Fall 2014
· Organized class materials and previous test materials to support members		
Executive Vice President	10 hours/week	Fall 2015
· Managed all lower chair positions in fulfilling commitments		
· Planned and organized fraternity events (social, professional, pledge, internal, fundraising, publicity)		